

# Buoyant flow of CO<sub>2</sub> through and around a semi-permeable layer of finite extent

Tri Dat Ngo<sup>1,†</sup>, Emmanuel Mouche<sup>1</sup> and Pascal Audigane<sup>2</sup>

<sup>1</sup>Laboratoire des Sciences du Climat et de l'Environnement, UMR 8212 CEA-CNRS-UVSQ, C.E. de Saclay, F-91191 Gif-sur-Yvette CEDEX, France

<sup>2</sup>Bureau des Recherches Géologiques et Minières, 3 Avenue Claude Guillemin – BP6009 – 45060 Orléans CEDEX 1, France

(Received 10 April 2016; revised 4 August 2016; accepted 16 October 2016;  
first published online 15 November 2016)

The buoyancy- and capillary-driven counter-current flow of CO<sub>2</sub> and brine through and around a semi-permeable layer is studied both numerically and theoretically. The continuities of the capillary pressure and the total flux at the interface between the permeable matrix and layer control the CO<sub>2</sub> saturation discontinuity at the interface and the balance between the buoyant and capillary diffusion fluxes on each side of the interface. This interface process is first studied in a one-dimensional (1-D) vertical column geometry using the concept of extended capillary pressure and a graphical representation of the continuity conditions in the  $(S_L, S_U)$  plane, where  $S_L$  and  $S_U$  are the lower and upper saturation traces at the interface, respectively. In two dimensions, we heuristically extend the two-phase gravity current model to the case where the current is bounded by a semi-permeable layer. Consequently, the current is not saturated with CO<sub>2</sub>, and its saturation and shape are derived from the flux and capillary pressure continuity conditions at the interface. This simplified model, which depends on CO<sub>2</sub> saturation only, is compared to fine grid simulations in the capillary-free and gravity-dominant cases. A good agreement is obtained in the second case; the current geometrical characteristics are accurately described. In the capillary-free case, we demonstrate that the local total velocity, which is, on average, zero because the flow is counter-current, must be considered in the total flux at the interface to obtain the same level of agreement.

**Key words:** gravity currents, multiphase flow, porous media

## 1. Introduction

Geological storage of carbon dioxide (CO<sub>2</sub>) is considered to be a pragmatic solution for the mitigation of global warming by reducing CO<sub>2</sub> emissions from large and concentrated sources. The sequestration of CO<sub>2</sub> is expected to be guaranteed during an extremely long time period by four basic trapping mechanisms: structural or stratigraphic, residual, solubility and mineral trapping (Benson *et al.* 2005; Celia *et al.* 2015). In a deep saline heterogeneous aquifer the structural and residual trappings should be the dominant mechanisms during the injection and the short-

<sup>†</sup> Email address for correspondence: [tridatxf@gmail.com](mailto:tridatxf@gmail.com)

medium-term post-injection periods. Injected at the bottom of this reservoir, and far from the injection well, the supercritical CO<sub>2</sub> rises buoyantly due to its difference in density with the reservoir brine. When the plume reaches a low-permeability layer, it spreads beneath as a gravity current and continues its buoyant rise at the layer ends until it reaches another layer or the cap-rock at the top of the reservoir (Huppert & Neufeld 2014). Consequently, the layers act as flow barriers and disperse the CO<sub>2</sub> plume, which increases the plume volume and the CO<sub>2</sub> residual trapping. This stratification process is currently observed at the pilot site in Sleipner where CO<sub>2</sub> has been injected into the Utsira aquifer since 1996 (Bickle *et al.* 2007).

The gravity current model used by several authors to describe the CO<sub>2</sub> currents relies on two assumptions (Huppert & Woods 1995): (i) the CO<sub>2</sub> and the brine are completely segregated and separated by a sharp interface; and (ii) the pressure in the CO<sub>2</sub> current is hydrostatic and its flow is principally parallel to the layer horizontal boundary and driven by the gradient of the current thickness. These assumptions are valid as long as the capillarity is neglected and the current thickness is considerably smaller than its lateral extent. This vertical equilibrium approximation, similar to the Dupuit–Forchheimer assumption in hydrology (Bear 1988), has proven to be fruitful to model different sequestration situations and scenarios. This result is partly due to the self-similar properties of the equation governing the gravity current thickness, which allows for analytical solutions to be determined when boundary conditions are appropriate (Huppert & Woods 1995). Gravity current models have been applied to CO<sub>2</sub> injection in homogeneous horizontal confined aquifers, in two dimensions (Huppert & Woods 1995; Nordbotten & Celia 2006; Hesse *et al.* 2007), in 3-D axisymmetric geometries (Lyle *et al.* 2005) and in 2-D sloping confined aquifers (Vella & Huppert 2006). They have also been used, for instance, to assess the CO<sub>2</sub> footprint in an aquifer by considering the residual trapping mechanism (Hesse, Orr & Tchelepi 2008; Juanes, MacMinn & Szulczewski 2010), the dispersion of a CO<sub>2</sub> plume in a 2-D periodic array of low-permeability layers (Hesse & Woods 2010) or the CO<sub>2</sub> stratification beneath shale layers at the Sleipner site (Bickle *et al.* 2007). For more applications, one can refer to the reviews of Huppert & Neufeld (2014) and Celia *et al.* (2015). When the capillarity is considered, the classical gravity current assumptions are not valid. Because of capillary diffusion, there is no longer a sharp interface, however a transition zone exists between the two fluids. Golding *et al.* (2011) extended the vertical equilibrium approach to the capillary case and proposed a two-phase gravity current model. These authors performed a sensitivity analysis of the current characteristics with respect to the Bond number, which provides a measure of the importance of capillarity compared to buoyancy. Later, the model was extended to the axisymmetric geometry (Golding, Huppert & Neufeld 2013). Different authors applied the single-phase current approach to the case in which the low-permeability layers, or the cap-rock, allowed the CO<sub>2</sub> to leak (Pritchard, Woods & Hogg 2001; Neufeld & Huppert 2009; Woods & Farcas 2009). Thus, they used the drainage approximation, in which the current remains in single phase and is governed by vertical equilibrium. In its simplest form, this leads to a gravity current equation with a source term proportional to the current height. Here, there is a strong analogy with certain hydrological problems, such as modelling an unconfined leaky aquifer (Bear 1988).

The single-phase approximation is no longer justified for a two-phase flow problem in a domain with a permeable matrix and a semi-permeable layer. This type of layer generally has a permeability of approximately one-tenth of the matrix permeability whereas a low-permeability layer has a permeability of approximately one hundredth

or less. In a deep heterogeneous saline aquifer, the type of heterogeneity depends on the geological formation, studied facies and scale of investigation. In an aquifer such as Utsira at the Sleipner site, the kilometric mudstone layers are low-permeability units (Bickle *et al.* 2007) whereas in other potential aquifers, the permeability contrast between the matrix and the heterogeneities may be less pronounced. This issue, which is site specific and scale dependent, is beyond the scope of this study and discussions may be found in Ambrose *et al.* (2008) or Lengler, De Lucia & Kühn (2010). When the permeability of the layer becomes non-zero, the phase segregation is incomplete, the CO<sub>2</sub> and the brine can pass through the layer and the CO<sub>2</sub> saturation in the current decreases while the permeability of the layer increases. The presence of the brine in the current and the two-phase flow at the interface between the matrix and the layer must be considered in the model. This is particularly true when the flow is counter-current: the CO<sub>2</sub> ascending flow rate across a horizontal section of the domain is balanced by the descending brine flow rate. The counter-current flow corresponds to the inject-low-and-let-rise strategy, which aims to increase the residual trapping (Bryant, Lakshminarasimhan & Pope 2008).

When the layers of a reservoir have a low permeability, such as at the Sleipner site, the CO<sub>2</sub> can sweep only a very limited volume of the reservoir: the gravity currents domain beneath the layers and the cap-rock, and the CO<sub>2</sub> chimneys at the layer extremities. When the layers are semi-permeable the CO<sub>2</sub> can sweep a much larger region as the CO<sub>2</sub> can pass through the layers. This may have an important impact on the sequestration properties of the reservoir, and principally on its trapping efficiency. Two short-term or mid-term trapping mechanisms are distinguished in the literature: capillary trapping and CO<sub>2</sub> dissolution in the brine (Benson *et al.* 2005). Capillary trapping is a post injection mechanism and takes place principally at the trailing edge of the plume where blobs of CO<sub>2</sub> are trapped in the reservoir pores (Doughty 2007; Hesse *et al.* 2008). The amount of trapped CO<sub>2</sub> increases with the saturation in the plume. Therefore, this amount should be locally high in the high saturation regions described previously and low in the rest of the reservoir, as the saturation of CO<sub>2</sub> flowing out the layers is expected to be low. Nevertheless, at the scale of the reservoir the global amount of trapped CO<sub>2</sub> should be much more important than if layers were impermeable. The second trapping mechanism, CO<sub>2</sub> dissolution, should be also enhanced as it depends on the contact volume between CO<sub>2</sub> and brine (Huppert & Neufeld 2014). Dissolution is expected to give rise to mineral trapping which is considered as a long-term trapping mechanism (Benson *et al.* 2005).

In this paper, we study this problem by considering the 2-D flow around and through a single semi-permeable layer of finite extent embedded in a permeable matrix. We consider three forces: buoyancy, capillarity and viscosity. There is no injection and the flow is counter-current at the scale of the reservoir, i.e. not at the local scale. The flow dynamics is essentially ruled by the interface conditions: capillary pressure continuity and total flux continuity at the layer matrix interface. In § 2, we recall the equations of the incompressible immiscible two-phase flow model, and we investigate this interface problem for a 1-D geometry (§ 3): a vertical column consisting of a piecewise homogeneous porous medium. Based on the studies performed by Cancès (2010*a,b*) and Andreianov & Cancès (2013), we demonstrate how to graphically determine the saturation discontinuity at the interface and the steady state saturation distributions in each domain of the column from the capillary and buoyant flux curves. In § 4, the 2-D problem is considered. Hence, we heuristically extend the model proposed by Golding *et al.* (2011) to the case of a semi-permeable layer.

We separately consider the capillary-free and the gravity-dominant cases. The proposed model is compared to fine grid numerical simulations performed using DuMu<sup>x</sup>, which is an open-source simulator for flow and transport processes in porous media developed by the University of Stuttgart (Flemisch *et al.* 2011). The comparison indicates that the model adequately describes the flow dynamics; however, in the capillary-free case, it also demonstrates that the total velocity fluctuations, which, on spatial averaging are zero, should be considered in the total flux function at the interface to improve the accuracy of the gravity current prediction.

## 2. Two-phase incompressible, immiscible flow model

The governing equations of two-phase incompressible, immiscible flow in a porous medium are given by Darcy's law and the mass conservation equation (Helmig 1997)

$$\mathbf{q}_\alpha = -\frac{kk_{r_\alpha}}{\mu_\alpha}(\nabla p_\alpha + \rho_\alpha \mathbf{g}), \quad \alpha = nw, w, \quad (2.1)$$

$$\phi \frac{\partial S_\alpha}{\partial t} + \nabla \cdot \mathbf{q}_\alpha = \mathcal{S}_\alpha, \quad \alpha = nw, w, \quad (2.2)$$

where the subscripts  $w$  and  $nw$  denote the wetting (brine) and the non-wetting (CO<sub>2</sub>) phases, respectively;  $S_\alpha$  (–),  $\mathbf{q}_\alpha$  (L/T) and  $\mathcal{S}_\alpha$  (L/T) are the saturation, the Darcian velocity and the sink/source terms of the phase  $\alpha$ , respectively;  $\mathbf{g}$  (L/T<sup>2</sup>) is the gravity acceleration vector;  $\phi$  (–) is the porosity;  $k$  (L<sup>2</sup>) is the absolute permeability of the porous medium; and  $p_\alpha$  (M/(LT<sup>2</sup>)),  $\rho_\alpha$  (M/L<sup>3</sup>),  $\mu_\alpha$  (M/(LT)) and  $k_{r_\alpha}$  (–) are the pressure, the density, the viscosity and the relative permeability of the phase  $\alpha$ , respectively. The relative permeabilities are considered as functions of the phase saturations only and can be given by the simplified Brooks and Corey's formulas as follows

$$k_{r_w} = (1 - S_{nw_e})^2, \quad (2.3)$$

$$k_{r_{nw}} = S_{nw_e}^2, \quad (2.4)$$

where  $S_{nw_e}$  is the normalized non-wetting saturation, defined by

$$S_{nw_e} = \frac{S_{nw} - S_{nw_r}}{1 - S_{w_r} - S_{nw_r}}, \quad (2.5)$$

with  $S_{\alpha_r}$  is the residual saturation of phase  $\alpha$ . The normalized saturations of the wetting and non-wetting phases sum up to one:  $S_{w_e} + S_{nw_e} = 1$ . In what follows, the normalized saturation of the non-wetting phase  $S_{nw_e}$  is written as  $S$  for simplicity. Thus, (2.3) and (2.4) become

$$k_{r_w}(S) = (1 - S)^2, \quad (2.6)$$

$$k_{r_{nw}}(S) = S^2. \quad (2.7)$$

The difference in the phase pressures is the capillary pressure

$$p_c(S) = p_{nw} - p_w. \quad (2.8)$$

The capillary pressure is typically viewed as a function of the wetting saturation and can be given by either a Van Genuchten (Van Genuchten 1980) or a Brooks and Corey

(BC) (Brooks & Corey 1964) function. In this paper, only a BC capillary pressure expression is considered

$$p_c(S) = \sigma \sqrt{\frac{\phi}{k}} J(S), \tag{2.9}$$

where  $J(S) = (1 - S)^{-1/\lambda}$  is the Leverett’s function, which is based on the saturation of the non-wetting phase and the pore size distribution parameter  $\lambda$ ; and  $\sigma$  (M/(LT<sup>2</sup>)) is the interfacial tension between the phases. Here, we assume  $\lambda = 2$ , which is a standard choice in porous media studies. The entry pressure corresponds to the capillary pressure value when  $S = 0$

$$p_e = p_c(S = 0) = \sigma \sqrt{\frac{\phi}{k}}. \tag{2.10}$$

The hysteresis in the capillary pressures and the relative permeabilities curves are neglected, and the same capillary pressure function is used for both the imbibition and drainage processes.

By combining (2.1) and (2.8), the Darcian velocity of the non-wetting phase can be written as

$$\mathbf{q}_{nw} = \mathbf{q}_t f(S) + \frac{k}{\mu_w} \Lambda(S) (\Delta \rho \mathbf{g} - \nabla p_c), \tag{2.11}$$

where  $\mathbf{q}_t$  is the total velocity, which can be expressed as

$$\mathbf{q}_t = \mathbf{q}_w + \mathbf{q}_{nw}, \tag{2.12}$$

$$f(S) = \frac{k_{r_{nw}}(S)}{k_{r_{nw}}(S) + M k_{r_w}(S)}, \tag{2.13}$$

and

$$\Lambda(S) = \frac{k_{r_{nw}}(S) k_{r_w}(S)}{k_{r_{nw}}(S) + M k_{r_w}(S)}, \tag{2.14}$$

with  $M = \mu_{nw}/\mu_w$ , i.e. the viscosity ratio, and  $\Delta \rho = \rho_w - \rho_{nw}$ . The fractional flux function  $f(S)$  (2.13) is a monotonic increasing S-shaped function (Helmig 1997) whereas the gravitational flux function  $\Lambda(S)$  (2.14) has a bell-shaped form (Hayek, Mouche & Mügler 2009). By substituting (2.11) into (2.2), we obtain the non-wetting phase saturation transport equation

$$\phi \frac{\partial S}{\partial t} + \nabla \cdot \Phi = 0, \tag{2.15}$$

where the total flux of the non-wetting phase  $\Phi$  is

$$\Phi = \mathbf{q}_t f(S) + \frac{k}{\mu_w} \Lambda(S) \Delta \rho \mathbf{g} - \frac{k}{\mu_w} \Lambda(S) \nabla p_c. \tag{2.16}$$

The first term of the total flux is a convective flux, called viscous flux when produced by injection or pumping. The second term is the gravitational flux, which is also known as the buoyant flux and induced by the difference in the phase densities. The

last term is the capillary flux, which is provoked by the difference in pressure across the phases interface at the pore scale. In the sequel, we denote  $\mathbf{G}$  the gravitational flux

$$\mathbf{G}(S) = \frac{k}{\mu_w} \Lambda(S) \Delta \rho g. \quad (2.17)$$

We intentionally simplified the model to keep the discussion general and simple. The relative permeability functions could be more complex than Brooks and Corey's laws with an exponent equal to two. However, Brooks–Corey model is often used in petroleum engineering and the exponent depends generally on the geology of the reservoir (Honarpour, Koederitz & Herbert 1986). Adopting such quadratic relative permeabilities as (2.6) and (2.7) with a viscosity ratio  $M = 1$  results in a symmetric buoyant flux function  $\Lambda(S)$  with respect to the saturation  $S$ . Using a given viscosity ratio  $M \neq 1$  or another relative permeability law would lead to an asymmetry of  $\Lambda(S)$  and change the value of the different key saturations subsequently introduced in the paper, but not the dynamics. The important property conserved whatever the relative permeabilities is the bell shape of the buoyant flux function  $G(S)$  and its scale dependency with the permeability. Furthermore, it is worth noting that hysteresis is an important process in carbon sequestration studies but its inclusion into a model makes both the physics and numerics more complex (Doughty 2007). We discuss in the conclusion (§ 6) the effect of this process on the trapping efficiency of a reservoir.

### 3. CO<sub>2</sub> buoyant migration in a vertical column filled with a piecewise homogeneous porous medium

To study the flow of CO<sub>2</sub> through the interface between two porous media, we first consider a 1-D vertical  $H$  (m) height column filled with a piecewise homogeneous porous medium consisting of two materials, permeable and semi-permeable. The interface  $\Gamma$  is located at  $z = 0$  m (figure 1). For simplicity, only the absolute permeability is heterogeneous:  $k^+$  for the permeable material and  $k^-$  for semi-permeable material, with a permeability ratio  $k^-/k^+ = 1/2$ . The other material parameters are constant in the column. Moreover, we henceforth assume that the CO<sub>2</sub> and brine viscosities are identical. This assumption is introduced to make the discussion simple but does not alter the results or the following discussions. The impact of the viscosity ratio on the flow dynamics is discussed further in § 3.4. We consider a counter-current flow,  $\mathbf{q}_i = 0$ , which indicates that there is no phase injection or pumping in the column. The non-wetting phase rises buoyantly upwards whereas the wetting phase flows downwards, and the volume in the first phase is replaced by the same volume of the second phase. The entire column is initially saturated with brine, and a constant non-wetting phase saturation is imposed at the bottom of the column which corresponds to an imposed buoyant flux value. A zero non-wetting saturation is imposed at the top to allow the CO<sub>2</sub> phase to migrate freely upwards (figure 1). We denote  $k_i$ ,  $G_i$  and  $\Phi_i$  as the absolute permeability, gravitational flux and total flux function in the material  $i$ , ( $i \in [l, u]$ ), respectively, where the subscripts  $l$  and  $u$  denote the lower and upper materials, respectively.

The 1-D hydrodynamics of a two-phase mixture at the interface of such a discontinuous medium under the simultaneous effects of the capillary and gravity forces has rarely been studied in the literature. A few authors considered either buoyancy (Langtangen, Tveito & Winther 1992; Kaasschieter 1999; Adimurthi, Jaffré & Veerappa Gowda 2004) or capillarity alone (Van Duijn & De Neef 1998). Others

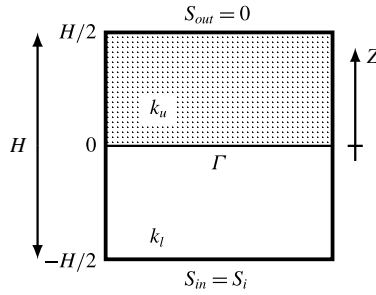


FIGURE 1. Sketch of the piecewise homogeneous porous medium column.

studied the effects of capillarity in the viscous case but disregarded buoyancy, i.e. when one phase is injected at the inlet of a horizontal column (Van Duijn, Molenaar & De Neef 1995; Mikelic, van Duijn & Pop 2002; Buzzi, Lenzinger & Schweizer 2009). Cancès (2010a,b) considered both capillarity and buoyancy. He proved the existence of a weak solution that satisfies the total flux continuity and the capillary pressure matching condition at the interface between the two media. However, this author did not study the effects of the materials permeabilities and the inflow rate of the buoyant phase on the saturation distribution in the column.

3.1. One-dimensional vertical migration model and continuity conditions at the interface

Using (2.15) and (2.16), the CO<sub>2</sub> saturation transport equation in the vertical column is written as

$$\phi \frac{\partial S}{\partial t} + \frac{\partial}{\partial z} \left\{ \frac{k(z)}{\mu_w} \Lambda(S) \left( \Delta\rho g - \frac{\partial p_c}{\partial z} \right) \right\} = 0. \tag{3.1}$$

To express this equation in a dimensionless form, we set the column height  $H$  as the characteristic length scale and the time  $T = (\phi H \mu_w) / (k_0 g \Delta\rho)$  for the CO<sub>2</sub> to migrate buoyantly in a column filled only with the permeable material as the characteristic time. The intrinsic permeability  $k^+$  is set as the permeability scale  $k_0$  of the medium.

$$z \equiv \frac{z}{H}, \quad k(z) \equiv \frac{k(z)}{k_0}, \quad t \equiv \frac{t}{T}. \tag{3.2a-c}$$

These scalings lead to the capillary number  $N_c$

$$N_c = \frac{\sigma}{g \Delta\rho H} \sqrt{\frac{\phi}{k_0}} = \frac{p_e}{g \Delta\rho H}. \tag{3.3}$$

Then, the dimensionless transport equation can be written as

$$\frac{\partial S}{\partial t} + \frac{\partial}{\partial z} \left\{ k(z) \Lambda(S) \left( 1 - \frac{N_c}{\sqrt{k(z)}} J'_s \frac{\partial S}{\partial z} \right) \right\} = 0, \tag{3.4}$$

where  $J'_s = dJ/ds$ . When the capillarity is neglected ( $N_c = 0$ ), the flux contains only the gravitational part and the (3.4) reduces to the well-known Buckley–Leverett equation with gravity (Kaasschieter 1999)

$$\frac{\partial S}{\partial t} + \frac{\partial G(S)}{\partial \hat{z}} = 0, \tag{3.5}$$

where

$$G(S) = k(z)\Lambda(S) \quad (3.6)$$

is the scaled gravitational flux.

The dynamics of the two-phase flow depends on the value of  $N_c$ . The dynamics may be classified into four different flow regimes: capillarity dominant ( $N_c \gg 1$ ), balance case ( $N_c \approx 1$ ), gravity dominant ( $N_c \ll 1$ ) and capillarity free ( $N_c = 0$ ). When  $N_c \geq 1$ , the capillarity leads to pseudo-linear  $\text{CO}_2$  saturation distributions in each material of the column. This case is not considered here and will be discussed in a forthcoming paper. The capillarity-free case has been studied by Hayek *et al.* (2009) in the framework of the theory of shocks and rarefaction waves. The authors demonstrated that the continuity of the buoyant flux  $G(S)$  at the interface leads to a saturation discontinuity and, in certain conditions, a  $\text{CO}_2$  stratification beneath the interface. This stratification can be qualified as a 1-D gravity current, and the phase segregation resulting in 2-D or 3-D gravity currents may be interpreted as a shock travelling in the direction of the gravity balanced by a lateral spreading of the saturation. Furthermore, the purely capillary case (no buoyancy) results in a saturation discontinuity (Van Duijn & De Neef 1998). Here, the case of interest is the gravity-dominant flow with a low positive capillary number  $N_c \ll 1$ . As presented in the next section, based on the arrangement of the materials in the column ( $k_l, k_u$ )  $\equiv (k^-, k^+)$  or ( $k_l, k_u$ )  $\equiv (k^+, k^-)$ , the buoyancy and capillarity may generate a  $\text{CO}_2$  stratification beneath the interface. Regardless of this arrangement, the difference in the entry capillary pressures between the two materials results in a  $\text{CO}_2$  saturation discontinuity at the interface. The one-sided traces of saturation at the interface, known as  $S_L$  and  $S_U$  with subscripts  $L$  and  $U$  denoting the lower and upper sub-domains, respectively, must fulfil two conditions: the continuity of the capillary pressure and the continuity of the total flux, which latter are expressed as follows

$$k_l \cdot \Lambda(S_L) \cdot \left(1 - \frac{N_c}{\sqrt{k_l}} \cdot J'_s \cdot \frac{\partial S_L}{\partial z}\right) = k_u \cdot \Lambda(S_U) \cdot \left(1 - \frac{N_c}{\sqrt{k_u}} \cdot J'_s \cdot \frac{\partial S_U}{\partial z}\right). \quad (3.7)$$

When the capillarity disappears, the condition of the total flux continuity is reduced to only that of the gravitational flux

$$k_l \cdot \Lambda(S_L) = k_u \cdot \Lambda(S_U). \quad (3.8)$$

This limit, known as the vanishing capillarity limit, has been studied from a mathematical point of view by Andreianov & Cancès (2013). For ( $k_l, k_u$ )  $\equiv (k^+, k^-)$ , the matching condition of capillary pressure results in the threshold saturation  $S^*$

$$p_c^+(S^*) = p_c^-(0) \Leftrightarrow \frac{J(S^*)}{\sqrt{k^+}} = \frac{J(0)}{\sqrt{k^-}}. \quad (3.9)$$

A natural way to connect the capillary pressures at the interface between layers is to define the multi-valued capillary pressure function. This definition has been introduced by Cancès, Gallouët & Porretta (2009) and Buzzi *et al.* (2009) to study of discontinuous-flux problems. Using the notations defined by these authors, the extended capillary pressure function can be written as

$$\bar{p}_c(S) := \begin{cases} \sigma \sqrt{\frac{\phi}{k(z)}} J(S) & \text{if } 0 < S < 1, \\ (-\infty, p_{c,\min}] & \text{if } S = 0, \\ [p_{c,\max}, +\infty) & \text{if } S = 1, \end{cases} \quad (3.10)$$



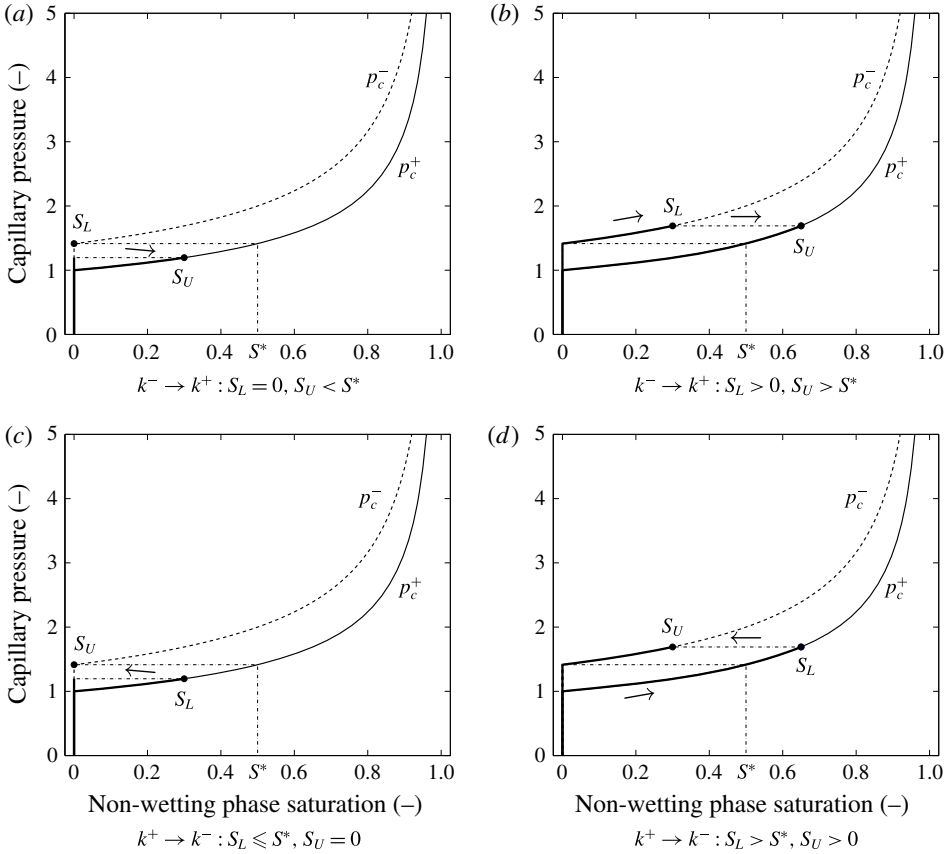


FIGURE 2. Capillary pressure curves of the materials  $k^+$ ,  $p_c^+$  and  $k^-$ ,  $p_c^-$ , and paths of  $(S_L, S_U)$  for the cases  $k^- \rightarrow k^+$  (a,b) and  $k^+ \rightarrow k^-$  (c,d). The thick curves represent the connected parts of the capillary pressure curves.

where  $p_{c,min} = \lim_{S_w \searrow 0} p_c$  and  $p_{c,max} = \lim_{S_w \nearrow 1} p_c$ . Thus, the continuity of capillary pressure is expressed as

$$\bar{P}_{c,l}(S_L) \cap \bar{P}_{c,u}(S_U) \neq \emptyset. \tag{3.11}$$

Figure 2 illustrates the path of  $(S_L, S_U)$  on the capillary curves for the cases  $(k_l, k_u) \equiv (k^-, k^+)$  and  $(k_l, k_u) \equiv (k^+, k^-)$ , which is henceforth denoted by  $k^- \rightarrow k^+$  and  $k^+ \rightarrow k^-$ , respectively. In the first case,  $k^- \rightarrow k^+$ , when  $S_L = 0, S_U < S^*$  (figure 2a), and when  $S_U > S^*, S_L$  increases (figure 2b). In the second case,  $k^+ \rightarrow k^-$ , the paths of  $S_L$  and  $S_U$  are interchanged: when  $S_L < S^*, S_U = 0$  (figure 2c), and when  $S_L > S^*, S_U$  increases (figure 2d). Furthermore, these paths are constrained by the total flux continuity condition. To graphically observe the effects of this constraint on the couple  $(S_L, S_U)$ , the couple is represented on the gravitational flux curves for different values of  $(S_L, S_U)$  (figure 3). For simplicity, we assume that in figure 3, and henceforth, the CO<sub>2</sub> and brine viscosities are identical. This assumption is introduced to make the discussion simple but does not alter the results or the following discussions. The impact of the viscosity ratio on the flow dynamics is discussed further in § 3.4. Figure 3 shows that, for a given couple  $(S_L, S_U)$ , there is generally no continuity of

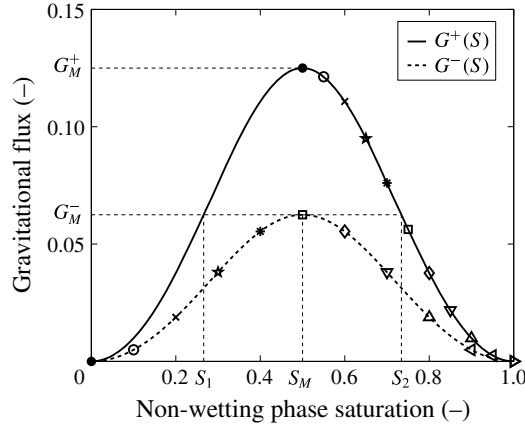


FIGURE 3. Gravitational fluxes  $G^-$  in the material  $k^-$  (dashed line) and  $G^+$  in the material  $k^+$  (continuous line). Each pair of markers plotted on these curves represents a couple  $(S_L, S_U)$  satisfying the capillary pressure continuity condition at the interface.  $G_M^-$  and  $G_M^+$  are the maximal gravitational fluxes in the layer and in the matrix respectively.  $S_M$  is the saturation in the layer such that  $G^-(S_M) = G_M^-$ ;  $S_1$  and  $S_2$  are the saturations in the matrix such that  $G^+(S_1) = G^+(S_2) = G_M^-$ .

the gravity flux. The difference is balanced by the capillary flux beneath the interface. The overall equilibrium at the interface depends on the value of the initial gravity flux. We examine now in detail the two cases  $k^- \rightarrow k^+$  and  $k^+ \rightarrow k^-$  for a permeability ratio of  $k^-/k^+ = 1/2$ , which results in a threshold saturation of  $S^* = 1/2$ . We simulate the transport of a  $\text{CO}_2$  plume generated by an imposed saturation  $S_i$  at the bottom of the column (figure 1). These simulations are performed with a home-made code based on the algorithm of Cancès (2008) using the Godunov discretisation scheme.

### 3.2. Case $k^- \rightarrow k^+$

Because the entry capillary pressure ratio is  $p_e^-/p_e^+ = \sqrt{2}$ , there is no capillary barrier. Therefore, when the  $\text{CO}_2$  plume reaches the interface between the two media, the plume immediately crosses the interface. The saturation traces  $S_L$  and  $S_U$  are determined from the total flux continuity condition and the value of the imposed saturation  $S_i$  at the bottom of the column. The total flux continuity,  $G^-(S_i) = \Phi^+(S_U) = G^+(S_U)$ , determines  $S_U$ . In the case of  $S_U \leq S^*$ ,  $S_L$  remains unchanged at zero, and the buoyant flux on the lower side of the interface is also equal to zero. Therefore, the total flux on this side is reduced to its capillary diffusion component. Figure 4(b) depicts the temporal evolution of the  $\text{CO}_2$  saturation distribution for  $S_i = 0.3$ . The buoyant flux curves displayed in figure 4(a) indicate that the upper saturation trace is  $S_U \approx 0.2$ . The apparent non-zero  $S_L$  value at  $t = 6.8$  is due to the finite difference discretisation scheme, where variables are assigned at the cell centres instead of the cell edges. The case  $S_U > S^*$  does not exist with our selection of parameters and relative permeability laws for which  $S^* = 1/2$ . This case is improbable if not impossible because (i) in most of the reservoirs,  $S^*$  is greater than the saturation  $S_M$  for which the buoyant flux is maximum, here  $S_M = 0.5$ , and (ii) the capillary pressure continuity implies that  $S_U > S_L$ , which indicates that  $S_U$  is greater than  $S_M$  and therefore describes a shock travelling downwards (Hayek *et al.* 2009).

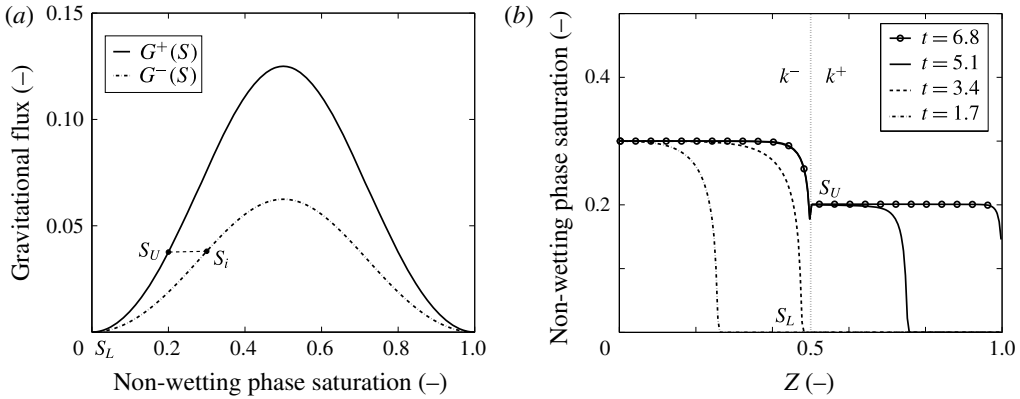


FIGURE 4. CO<sub>2</sub> migration in a vertical column filled with a piecewise homogeneous porous medium. (a) Gravitational fluxes  $G^-$  in the material  $k^-$  (dashed line) and  $G^+$  in the material  $k^+$  (continuous line). The couple  $(S_i, S_U)$  satisfies the gravitational flux continuity, where  $S_i$  is the imposed saturation at the bottom of the column. (b) Saturation distributions along the vertical axis of the column at four times. At  $t = 6.8$ , the saturation is at steady state.

### 3.3. Case $k^+ \rightarrow k^-$

The continuity of the capillary pressure is no longer automatically satisfied as in the previous case,  $k^- \rightarrow k^+$ . Therefore, the CO<sub>2</sub> accumulation occurs beneath the interface until  $S_L$  is equal to  $S^*$ . Beyond this value, CO<sub>2</sub> can flow through the interface, and the couple of saturation  $(S_L, S_U)$  satisfies the capillary pressure continuity (3.11) (figure 2c). Andreianov & Cancès (2013) indicated how to graphically determine this couple in the  $(S_L, S_U)$  plane using the solution curves  $S_U(S_L)$  of the capillary pressure continuity condition and the buoyant flux continuity relationship. Let us define  $\mathcal{P}$  as the curve  $S_U(S_L)$  solution of the capillary pressure continuity condition

$$\mathcal{P} := \{(S_L, S_U) \in [0, 1]^2 \mid p_c^+(S_L) \cap p_c^-(S_U) \neq \emptyset\}. \tag{3.12}$$

Furthermore,  $\mathcal{G}$  is defined as the solution curve  $S_U(S_L)$  of the buoyant flux relationship

$$\mathcal{G} := \{(S_L, S_U) \in [0, 1]^2 \mid G^+(S_L) \cap G^-(S_U)\}. \tag{3.13}$$

Curves  $\mathcal{P}$  and  $\mathcal{G}$  are plotted in figure 5. Due to the bell shape of the buoyant flux, curve  $\mathcal{G}$  consists of three branches:  $\mathcal{G}_1$  and  $\mathcal{G}_2$ , which correspond to  $(S_L < S_1, S_U < S_M)$  and  $(S_L > S_2, S_U < S_M)$ , respectively, and  $\mathcal{G}_3$ , which corresponds to  $(S_1 < S_L < S_2, S_U = S_M)$ , where  $S_M = 0.5$  is the saturation for which the gravitational flux is maximum, and  $S_1 = 0.265$  and  $S_2 = 0.735$  are the saturations such that  $G^+(S_1) = G^+(S_2) = G^-(S_M)$  with  $S_1 < S_2$  (figure 3). The couple  $\bar{S}_{LU} = (\bar{S}_2, \bar{S}_U)$  represented in figure 5 is the intersection point between the curves  $\mathcal{P}$  and  $\mathcal{G}$  in the  $(S_L, S_U)$  plane. This couple defines the maximum CO<sub>2</sub> flux that can cross the interface and respects the continuity conditions at the interface. The two saturations  $\bar{S}_1, \bar{S}_2$  in figure 5 are fortuitously close to  $S_1, S_2$ . This should not be the case with a different set of relative permeabilities and capillary pressure laws.

The saturation discontinuity and distribution in the column depends strongly on the imposed saturation  $S_i$  at the bottom of the column. Two cases must be distinguished:  $S_i \leq \bar{S}_1$ , i.e. the buoyant inflow flux is lower than the maximum flux, which can flow into the material  $k^-$ , and the inverse case.

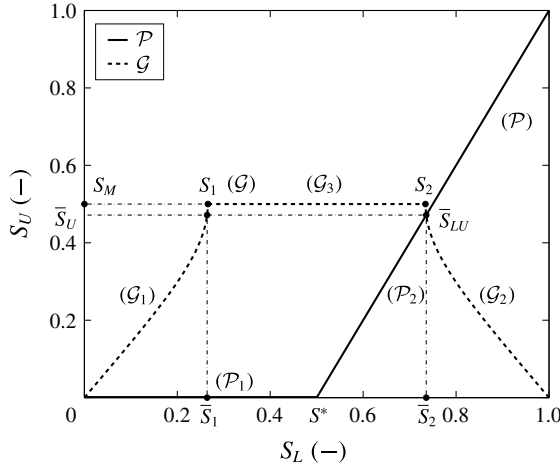


FIGURE 5. Curves  $S_U(S_L)$ , solutions of the capillary pressure continuity condition, curve  $\mathcal{P}$  (continuous line), and the gravitational flux continuity relationship, curve  $\mathcal{G}$  (dashed line). Curve  $\mathcal{P}$  is composed of two segments:  $\mathcal{P}_1$  for  $S_L \leq S^*$  and  $\mathcal{P}_2$  for  $S_L > S^*$ . Curve  $\mathcal{G}$  has three branches:  $\mathcal{G}_1$  and  $\mathcal{G}_2$  correspond to  $(S_L < S_1, S_U < S_M)$  and  $(S_L > S_2, S_U < S_M)$ , respectively, and  $\mathcal{G}_3$  to  $(S_1 < S_L < S_2, S_U = S_M)$ . The intersection point  $\bar{S}_{LU} = (\bar{S}_2, \bar{S}_U)$  of  $\mathcal{P}$  and  $\mathcal{G}$  is the steady state solution of the interface problem for  $S_i > \bar{S}_1$ , where  $G^+(\bar{S}_1) = G^+(\bar{S}_2) = G^-(\bar{S}_U)$  and  $\bar{S}_1 < \bar{S}_2$ .

To illustrate the first case,  $S_i \leq \bar{S}_1$ , we consider  $S_i = 0.15$  ( $\bar{S}_1 = 0.26$ ). The pathway showing the evolution of  $(S_L, S_U)$  towards their steady state values is depicted in figure 6(a), and the temporal evolution of the CO<sub>2</sub> saturation distribution in the column is depicted in figure 7(b). When the CO<sub>2</sub> plume reaches the interface, the capillary barrier results in an accumulation beneath the interface. The trace of saturation  $S_U$  is derived from the flux continuity condition. For any imposed saturation  $S_i \leq \bar{S}_1$ , there always exist a saturation  $S_U$  that satisfies the buoyant flux continuity relationship  $G^+(S_U) = G^-(S_i)$  (figure 6a). The imposed saturation value  $S_i = 0.15$  results in  $S_U = 0.22$  (figures 6a and 7a). The trace of saturation  $S_L$  is determined from the continuity of the capillary pressure at the interface:  $S_L = 0.61$ . The difference between the buoyant fluxes  $G^-(S_U)$  and  $G^+(S_L)$  is balanced by a capillary diffusion flux (figure 7b). It is important to note that the saturation traces  $(S_L, S_U)$ , and the gravitational flux difference  $G^+(S_L) - G^-(S_U)$  is thus not affected by a variation of the capillary number  $N_c$  (3.3). For the limit  $N_c \rightarrow 0$ , the saturation gradient beneath the interface increases, and the CO<sub>2</sub> peak shrinks and disappears when the capillary pressure tends to zero; hence, the capillary-free case is recovered.

In the second case,  $S_i > \bar{S}_1$ ,  $S_L$  increases until  $\bar{S}_2 = 0.74$  for which  $S_U = \bar{S}_U = 0.46$  (figure 6b). The difference between the initial buoyant flux  $G^+(S_i)$  and this maximum flux corresponds to a backward shock travelling at a velocity  $[G(S_i) - G(S_L)] / (S_i - S_L)$  (Hayek *et al.* 2009), as illustrated in figure 8(b).

### 3.4. Impact of the model parameters on the flow regime

For simplicity we assume in this work a viscosity ratio equal to one. For a viscosity ratio lying between  $10^{-1}$  and  $10^{-2}$ , which is the usual range for carbon sequestration studies (Huppert & Neufeld 2014), the position of the maximum flux is shifted

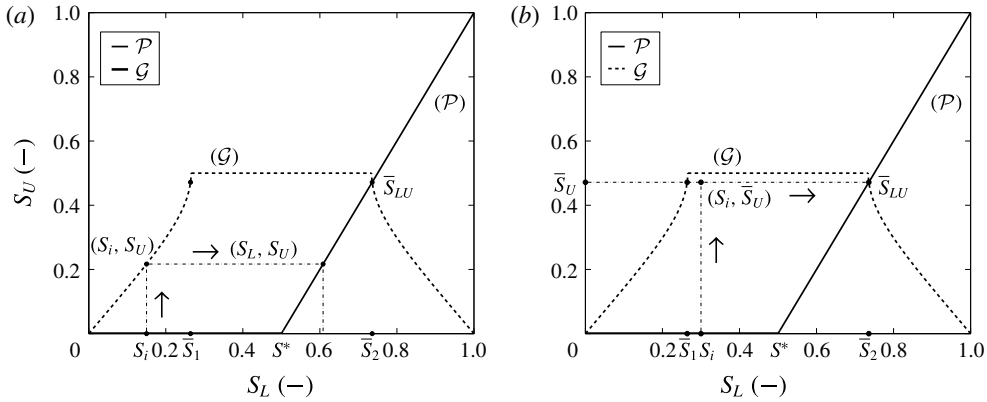


FIGURE 6. Curves  $S_U(S_L)$ , solutions of the capillary pressure continuity condition, curve  $\mathcal{P}$  (continuous line), and the gravitational flux continuity relationship, curve  $\mathcal{G}$  (dashed line) (see figure 5). The pathway to determine the steady state solution of the interface problem for  $S_i < \bar{S}_1$  (a) and for  $S_i \geq \bar{S}_1$  (b). The arrows indicate the direction of increasing  $S_L$  and  $S_U$ .

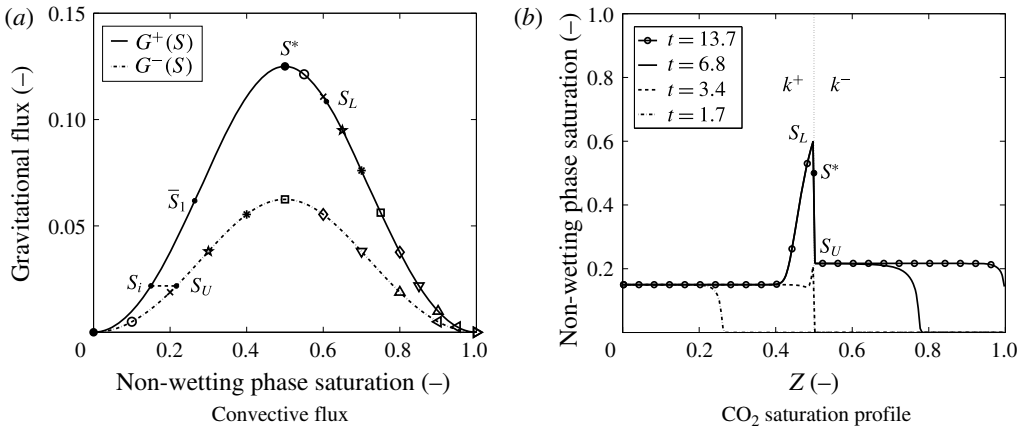


FIGURE 7. CO<sub>2</sub> migration in a vertical column filled with a piecewise homogeneous porous medium. (a) Gravitational fluxes  $G^-$  in the material  $k^-$  (dashed line) and  $G^+$  in the material  $k^+$  (continuous line). The couple  $(S_i, S_U)$  satisfies the capillary pressure continuity, where  $S_i$  is the imposed saturation at the bottom of the column. (b) Saturation distributions along the vertical axis of the column at four times. At  $t = 13.7$ , the saturation is at steady state.

towards  $S = 0$ . Using the notations of § 3.3 we have  $S_M = 0.25$  and  $G_M = 0.28$  for  $M = 0.1$ , whereas  $S_M = 0.5$  and  $G_M = 0.13$  for  $M = 1$ . Figures 9(a) and 9(b) display the buoyant flux curves with different values of the couple  $(S_L, S_U)$  for  $M = 0.1$  and  $M = 0.2$  respectively. In the case  $k^+ \rightarrow k^-$  and for  $S_i = 0.15$  we see that  $S_i > \bar{S}_1$  for  $M = 0.1$  ( $\bar{S}_1 = 0.13$ ) and  $S_i < \bar{S}_1$  for  $M = 0.2$  ( $\bar{S}_1 = 0.16$ ). According to the previous discussion (§ 3.3) the CO<sub>2</sub> accumulation beneath the interface tends to a steady state for  $M = 0.2$  and becomes unsteady for  $M = 0.1$ . We report on figures 9(a) and 9(b) the couples  $(S_L, S_U)$  for these two cases where  $(S_L = \bar{S}_2, S_U = \bar{S}_U)$  for  $M = 0.1$ .

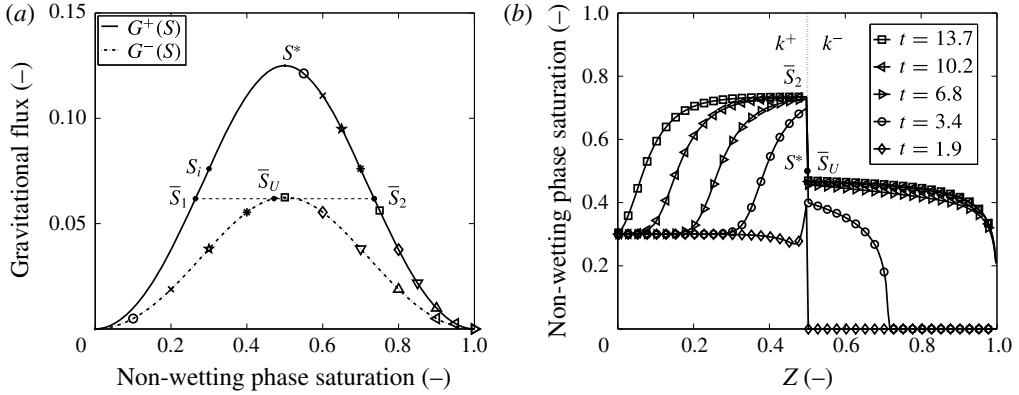


FIGURE 8. CO<sub>2</sub> migration in a vertical column filled with a piecewise homogeneous porous medium. (a) Gravitational fluxes  $G^-$  in the material  $k^-$  (dashed line) and  $G^+$  in the material  $k^+$  (continuous line). The couple  $\bar{S}_{LU} = (\bar{S}_L, \bar{S}_U)$  satisfies the capillary pressure and the gravitational continuity conditions and  $S_i$  is the imposed saturation at the bottom of the column. (b) Saturation distributions along the vertical axis of the column at five times. At  $t = 13.7$ , the saturation is at steady state.

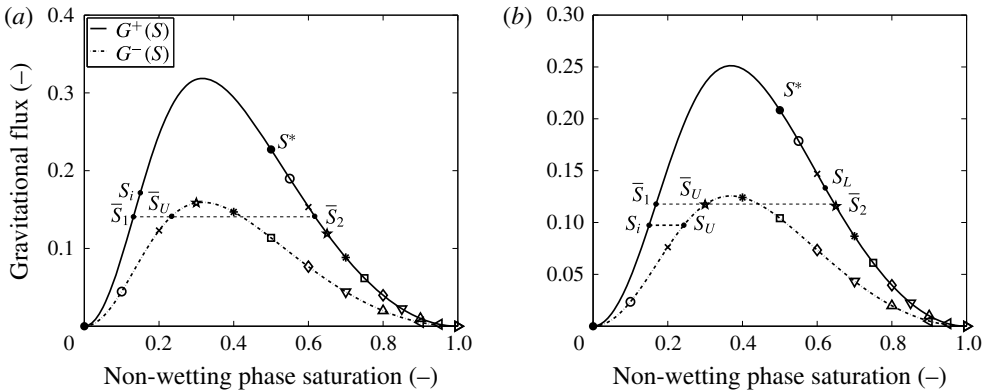


FIGURE 9. CO<sub>2</sub> migration in a vertical column filled with a piecewise homogeneous porous medium. Gravitational fluxes  $G^-$  in the material  $k^-$  (dashed line) and  $G^+$  in the material  $k^+$  (continuous line) for two values of the viscosity ratio  $M$ : (a)  $M = 0.1$ , (b)  $M = 0.2$ . The couple  $\bar{S}_{LU} = (\bar{S}_L, \bar{S}_U)$  satisfies the capillary pressure and the gravitational continuity conditions and  $S_i$  is the imposed saturation at the bottom of the column.

Figure 10 summarizes the three different flow regimes in the space described by the axis  $k_l/k_u$  and  $S_i$  for a given viscosity ratio. The saturation range is limited to  $(0, S_M)$  because any saturation greater than  $S_M$  cannot migrate upwards. The key parameter is  $\bar{S}_1$ , and it is easy to show that it depends on the ratio  $k^-/k^+$  and  $M$ .

#### 4. Gravity current model for a semi-permeable layer of finite extent

We now consider a 2-D reservoir consisting of a single horizontal semi-permeable layer of finite length  $2L$  embedded in a permeable matrix. The permeabilities of the matrix and the inclusion are  $k^+$  and  $k^-$ , respectively, with  $k^-/k^+ \ll 1$ . The reservoir, initially filled with brine, is fed by a uniform CO<sub>2</sub> buoyant flux generated by an

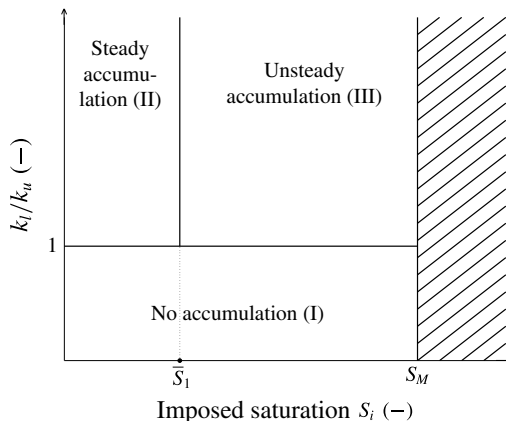


FIGURE 10. Flow regime diagram showing the three regimes of CO<sub>2</sub> accumulation beneath the interface as a function of the permeability ratio  $k_l/k_u$  and the imposed saturation  $S_i$  at the bottom of the column.

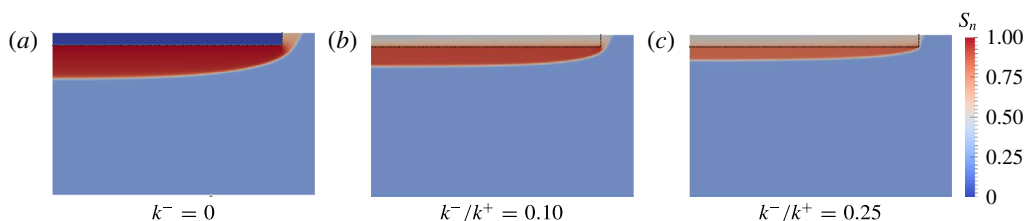


FIGURE 11. (Colour online) Simulation of the gravity currents ( $p_c = 0$ ) underlying an impervious (a) or a semi-permeable layer (b,c). The black lines delineate the interface between the matrix and the layer. Simulations are performed using the DuMu<sup>x</sup> code (Flemisch *et al.* 2011).

imposed CO<sub>2</sub> saturation at the bottom of the reservoir. The bottom is supposed to be far from the layer. Similar to the 1-D vertical column case studied previously in § 3, the flow is counter-current: the CO<sub>2</sub> ascending flow rate across a horizontal section of the reservoir is balanced by the descending brine flow rate. As there is no CO<sub>2</sub> injection the flow rate of the total velocity  $\mathbf{q}_t$  across the section (2.12) is zero but the velocity may be locally non-zero. This system could schematically represent the post-injection migration of a CO<sub>2</sub> plume in a single layer reservoir.

We study the buoyancy-dominant flow of CO<sub>2</sub> beneath and through the semi-permeable layer. The numerical simulations neglecting the capillary pressure indicate that this predominantly horizontal flow can be assimilated to a so-called gravity current driven by the density contrast between the CO<sub>2</sub> and the surrounding brine (figure 11). For permeability ratios  $k^-/k^+ \geq 0.1$ , figure 11 clearly indicates that there is a phase segregation and a neat interface between the gravity current and the remaining fluid. Furthermore, we can observe that when  $k^-/k^+$  increases, the CO<sub>2</sub> saturation in the gravity current  $S_{gc}$  decreases:  $S_{gc} \approx 0.9$  for  $k^-/k^+ = 0.1$  and  $S_{gc} \approx 0.8$  for  $k^-/k^+ = 0.25$ . The imposed saturation at the bottom of the reservoir is  $S_i = 0.25$ .

The extension of gravity current models to semi-permeable layers is a complex theoretical issue which is beyond the scope of the paper. Indeed, this extension must be able to describe the flows of brine and CO<sub>2</sub> in the gravity current, in the layer

and in the layer's surrounding, while respecting the phase segregation condition. The objective of our modelling approach is to simplify the problem by decoupling the flows of the two phases and to describe the flow of CO<sub>2</sub> by means of a single transport saturation equation with flux continuity conditions at the interfaces. For this purpose one must be able to circumvent the pressure equation, and therefore disregard the total velocity. Although this is not feasible in our 2-D problem one may hope that when flow is counter-current at the scale of the domain it is approximatively counter-current at the interfaces with the layer. Under this approximation the CO<sub>2</sub> vertical flow is one-dimensional and counter-current and the horizontal flow in the gravity current is governed by the horizontal gradient of the gravity current height. Adopting these assumptions we here propose to extend the gravity current models developed for impermeable layers to semi-permeable layers. These assumptions are discussed and heuristically justified in the appendix A.

Most of the studies on gravity currents in porous media use a sharp-interface approximation assuming that the regions within and without the current are fully saturated, and a macroscopic sharp interface exists between the two fluids (Huppert & Neufeld 2014). These single-phase gravity current models can only be applied when the capillary pressure is negligible compared to gravity and viscous forces. When capillarity is considered, the simulation indicates that both phases are present, and due to capillary diffusion, the vertical extent of the gravity current and its non-wetting phase saturation are greater and smaller, respectively, than that in the capillary-free case. Golding *et al.* (2011) developed a model that considers the capillary effect on the saturation distribution within the current. The authors proposed a vertically integrated model for a two-phase gravity current along a horizontal impermeable barrier, in which the local capillary effect is encapsulated directly into the total flux function. Thereafter, we extend their model to study the two-phase gravity current along a semi-permeable barrier of finite extent (appendix A).

The two-phase gravity current model beneath an impermeable boundary is based on the assumption of a vertical gravity–capillary equilibrium which expresses the balance between the gravitational and the capillary force within the current (Golding *et al.* 2011). We assume that this assumption is still valid when the boundary is semi-permeable (appendix A)

$$\frac{\partial p_c}{\partial z} = -\Delta\rho g, \quad (4.1)$$

where the vertical axis  $z$  is oriented downwards, and its origin is located at the centre of the low matrix inclusion interface. The relationship between the capillary pressure and the current height is determined by integrating equation (4.1) from  $z$  to the gravity current height  $h$  as follows

$$p_c[h(x, t), z] = p_e^+ (1 - S_h)^{-1/\lambda} - \Delta g(z - h), \quad (4.2)$$

where  $S_h$  denotes the non-wetting phase saturation at  $z = h$ , which is commonly equal to zero, except in our case where the gravity current is fed by a source distributed uniformly at the bottom of the reservoir, and  $p_e^+$  is the entry pressure of the permeable matrix. The expression of CO<sub>2</sub> saturation within the current as a function of the current height  $h$  and  $z$  is written as follows

$$S[h(x, t), z] = 1 - \left( (1 - S_h)^{-1/\lambda} + \frac{h - z}{h_e^+} \right)^{-\lambda}, \quad (4.3)$$



where  $h_e^+ = p_e^+ / \Delta\rho g$ . The non-wetting phase saturation  $S_0^+$  at  $z=0$  on the matrix side of the interface is

$$S_0^+ \equiv S_0^+(h/h_e^+) \equiv S[h(x, t), z=0] = 1 - \left( (1 - S_h)^{-1/\lambda} + \frac{h}{h_e^+} \right)^{-\lambda}. \tag{4.4}$$

A vertical integration of the mass conservation equation (2.2) for the non-wetting phase over the gravity current yields

$$\phi[S_0^+ - S_h] \frac{\partial h}{\partial t} - \frac{k^+ \Delta\rho g}{\mu_{nw}} \frac{\partial}{\partial x} \left[ h \frac{\partial h}{\partial x} \mathcal{F}(h/h_e^+) \right] = \Phi_{in} - \Phi_{out}, \tag{4.5}$$

where  $\Phi_{in}$ ,  $\Phi_{out}$  are the vertical feeding flux at  $z=h$  and the vertical leakage term at the interface, respectively, with the semi-permeable layer at  $z=0$ . The capillary effect on the gravity current is considered via the flux function  $\mathcal{F}(h/h_e^+)$

$$\mathcal{F}(h/h_e^+) \equiv \frac{\mu_{nw}}{h} \int_0^h \frac{k_{r_{nw}}(S(z))}{\mu_{nw}} dz = \frac{h_e^+}{\lambda h} \int_{S_h}^{S_0^+} S^2 (1 - S)^{-(\lambda+1)/\lambda} dS. \tag{4.6}$$

The current height at the layer ends is set to zero:  $h(x = \pm L) = 0$ . An analytical expression of  $\mathcal{F}$  is given by Golding *et al.* (2011) for  $S_h=0$ . Based on this expression, we derive

$$\mathcal{F}(h/h_e^+) = \frac{h_e^+}{h} [f(\lambda, S_0^+) - f(\lambda, S_h)], \tag{4.7}$$

where

$$f(\lambda, S) = \frac{(1 - S)^{-1/\lambda}}{1 - 2\lambda} \left[ S^2 + \frac{2\lambda(S - \lambda)}{\lambda - 1} \right] + \frac{2\lambda^2}{(\lambda - 1)(1 - 2\lambda)}. \tag{4.8}$$

The flux  $\Phi_{in}$  is assumed to be equal to the buoyant flux  $G^+(S_h)$ . At steady state, we have  $S_h = S_i$ , where  $S_i$  is the imposed saturation at the bottom of the reservoir. The saturation  $S_0^+$  on the matrix side of the interface between the low-permeability layer and the matrix and the flux  $\Phi_{out}$  are given by the buoyant flux and the capillary pressure continuity conditions at the interface. Based on the previous analysis of the CO<sub>2</sub> plume dynamics at the interface of a piecewise homogeneous porous medium (§ 3) the CO<sub>2</sub> can penetrate locally, i.e. for a given  $x$ , into the semi-permeable layer when the local capillary pressure in the gravity current at  $z=0$  exceeds the entry capillary pressure of the layer  $p_e^-$ . In terms of saturation, the vertical flow occurs locally if the local saturation  $S_0^+$  exceeds the threshold saturation  $S_0^*$  defined by (3.9). The relationship between  $S_0^+$  and the current height  $h$  expressed in (4.4) results in the notion of the threshold height  $h^*$

$$h^* = h_e^+ [(1 - S_0^*)^{-1/\lambda} - (1 - S_h)^{-1/\lambda}], \tag{4.9}$$

where  $S_0^*$  is a function of the permeability contrast  $k^-/k^+$ .

Woods & Farcas (2009) investigated the influence of the entry capillary pressure on the leakage of single-phase gravity currents through a low-permeability layer. However, in their study, the threshold height of the single-phase gravity current  $h^*$  is equal to  $h_e^-$ , and the impact of the permeability contrast between the matrix and the layer is not

studied. At steady state, Golding *et al.* (2011) introduced the dimensionless variables  $x = x/L$  and  $h = h/h_{gc}$ , where  $h_{gc}$  is the gravity current height scale corresponding to a steady state gravity current of the horizontal extent  $2L$ , which was originally introduced by Huppert & Woods (1995). In our system, this height scale is given as

$$h_{gc} = \sqrt{\frac{\Phi_{in}\mu_n L^2}{\Delta\rho g k^+}}. \quad (4.10)$$

Hence, the governing equation of the current height reads

$$\frac{\partial}{\partial x} \left[ h \frac{\partial h}{\partial x} \mathcal{F}(hB) \right] = \frac{\Phi_{out}}{\Phi_{in}} - 1 \quad \text{for } h \geq h^*, \quad (4.11)$$

and

$$\frac{\partial}{\partial x} \left[ h \frac{\partial h}{\partial x} \mathcal{F}(hB) \right] = -1 \quad \text{for } h < h^*, \quad (4.12)$$

where  $B$  is the Bond number

$$B = \frac{\Delta\rho g h_{gc}}{h_e^+}. \quad (4.13)$$

The solution of (4.11) and (4.12) depends strongly on the Bond number  $B$  and the capillary number  $N_c$ . Lastly, the dynamics of the system is essentially controlled by four variables or parameters: layer length  $2L$ , entry pressure in the matrix  $h_e^+$ , imposed saturation at the bottom of the reservoir  $S_i$  and ratio of the permeabilities  $k^-/k^+$ .

The outflux  $\Phi_{out}$  in (4.11) can be approximated by the buoyant flux on the inclusion side of the interface as follows

$$\Phi_{out} = G^-(S_0^-), \quad (4.14)$$

where the saturation  $S_0^-$  is the saturation on the inclusion side of the interface, which is determined via the matching condition of capillary pressure at this interface

$$p_c^-(S_0^-) = p_c^+(S_0^+), \quad (4.15)$$

where  $S_0^+$  is related to the height of the gravity current  $h$  via (4.4). In other words, the outflux  $\Phi_{out}$  is also a function of  $h$ . To determine  $h$ , equations (4.11) and (4.12) can be solved numerically using a predictor–corrector algorithm (Ames 2014).

When the capillarity is neglected,  $N_c = 0$ , unlike the single-phase gravity current beneath impermeable boundaries, the zone occupied by the current is not saturated with  $\text{CO}_2$  because of the leakage term  $\Phi_{out}$  through the layer. We can assume that at steady state, the saturation  $S_{gc}$  within the current is constant and determined from the continuity condition of the buoyant flux at the interface. We emphasize that in most of the works the flux  $\Phi_{out}$  is considered as a drainage term evaluated from the hydrostatic pressure assumption (Acton, Huppert & Worster 2001; Spannuth *et al.* 2009; Neufeld & Huppert 2009). This drainage assumption is not justified for a counter-current flow in a semi-permeable layer where the two-phase flow nature of the problem must be

respected. Finally, we recover the equation describing the propagation of current given by Huppert & Woods (1995) but with slight differences (appendix A)

$$\phi S_{gc} \frac{\partial h}{\partial t} - \frac{k^+ \Delta \rho g}{\mu_{nw}} \frac{\partial}{\partial x} \left[ k_{r_{mv}}(S_{gc}) h \frac{\partial h}{\partial x} \right] = \Phi_{in} - \Phi_{out}. \tag{4.16}$$

For the capillary case, we introduce the dimensionless variables  $x = x/L$  and  $h = h/h_{gc}$ , where the gravity current height scale  $h_{gc}$  is given by (4.10), in which  $k^+$  is replaced by  $k^+ k_{r_{mv}}(S_{gc})$  and  $\Phi_{in}$  is replaced by  $\Phi_{in} - \Phi_{out}$ . The profile of the single-phase gravity current at steady state is given by

$$\frac{\partial}{\partial x} \left[ h \frac{\partial h}{\partial x} \right] = -1, \tag{4.17}$$

where  $\Phi_{in} = G^+(S_i)$  and  $\Phi_{out} = G^+(S_{gc}) = G^-(S_{la})$ , with  $S_{la}$  denoting the saturation in the layer. Because the layer is thin, this saturation is assumed to be homogeneous. The solution of (4.17) is

$$h = \sqrt{1 - x^2}. \tag{4.18}$$

### 5. Numerical validation and discussion of the model

The reservoir introduced in the previous section is modelled as a rectangular domain with a width of  $2L_0 = 80$  m and a height of  $H = 100$  m with a length layer of  $2L = 72$  m localized at the centre and leaving two gaps of  $l = L_0 - L = 4$  m width on each side (figure 12). A CO<sub>2</sub> saturation  $S_i$  is imposed throughout the lower boundary of the domain which is initially saturated with brine. All of the other boundaries are impermeable and the brine is allowed to flow downwards through the lower boundary. The flow is counter-current: the brine initially located in the reservoir can flow downwards through the layer and the two gaps. This domain may be observed as the unit cell of a larger reservoir, which consists of a periodic array of identical horizontal layers with a length  $2L$  and a periodicity  $2L_0$ . The petrophysical parameters of the reservoir for the two studied cases, i.e. capillary free and gravity dominant, and the parameters of the fluids are summarized in table 1. For reasons explained in § 3.1, the brine and the CO<sub>2</sub> viscosities are assumed to be equal. The numerical validation of the model developed in the previous section is performed using DuMu<sup>x</sup>, which is an open-source simulator for the flow and transport processes in porous media developed by the University of Stuttgart (Flemisch *et al.* 2011). We successively discuss the cases without and with the capillarity. In this last case, we consider only the gravity-dominant flow,  $N_c \ll 1$ .

#### 5.1. Capillary-free case

We consider a permeability ratio  $k^-/k^+ = 1/10$  for the capillary-free case. The buoyant flux functions are depicted in figure 13. First, we emphasize that in the finite width domain considered here the buoyant flux imposed at the bottom is limited by a critical value beyond which a steady state gravity current cannot be obtained. This critical flux can be defined by the equality

$$\Phi_c = 2l \cdot G_M^+ + 2L \cdot G_M^-, \tag{5.1}$$

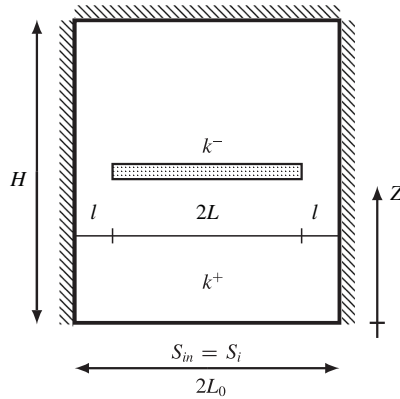


FIGURE 12. Reservoir with a single embedded layer of permeability  $k^-$  in a permeable matrix of permeability  $k^+$ .

		Capillary-free case	Gravity-dominant case $N_c = 0, 0.01, 0.1$
Permeability of matrix	( $\text{m}^2$ )	$3 \times 10^{-12}$	$3 \times 10^{-12}$
Permeability of layer	( $\text{m}^2$ )	$3 \times 10^{-13}$	$3 \times 10^{-13}$ ( $7.5 \times 10^{-13}$ )
Entry capillary pressure of matrix $p_e^+$	(Pa)	0	51 012
Entry capillary pressure of layer $p_e^-$	(Pa)	0	0, 16 131, 161 314 (0, 10 202, 102 024)
Porosity $\phi$	(—)	0.35	0.35
Density of brine $\rho_w$	( $\text{kg m}^{-3}$ )	1000	1000
Density of $\text{CO}_2$ $\rho_{nw}$	( $\text{kg m}^{-3}$ )	480	480
Viscosity of brine $\mu_w$	(Pa s)	$8 \times 10^{-4}$	$8 \times 10^{-4}$
Viscosity of $\text{CO}_2$ $\mu_{nw}$	(Pa s)	$8 \times 10^{-4}$	$8 \times 10^{-4}$
Pore size distribution parameter $\lambda$	(—)	2.0	2.0

TABLE 1. Parameters for the simulations of the capillary-free and gravity-dominant cases.

where  $G_M^+$  and  $G_M^-$  are the maxima of the buoyant flux in the matrix and the layer respectively (figure 13). This equality defines a critical saturation  $S_c$  given by the relationship

$$G^+(S_c) = \frac{\Phi_c}{2l + 2L}. \quad (5.2)$$

It is easy to find that the saturation  $S_1$  defined by  $G^+(S_1) = G_M^-$  and shown in figure 13 is always lower than the critical saturation  $S_c$ . The saturation  $S_1$  is the maximum saturation below which there is no gravity current, i.e. all of the imposed buoyant flux can pass through the layer. When  $k^- \rightarrow k^+$  we have  $S_1 \rightarrow S_c \rightarrow S_M$ . For  $k^-/k^+ = 1/10$  we have  $S_c = 0.156$  and  $S_1 = 0.112$ , and for  $k^-/k^+ = 1/4$ ,  $S_c = 0.205$  and  $S_1 = 0.180$ . Therefore, based on the continuity condition of the buoyant flux, three cases  $\mathcal{C}(1,2,3)$  must be identified:

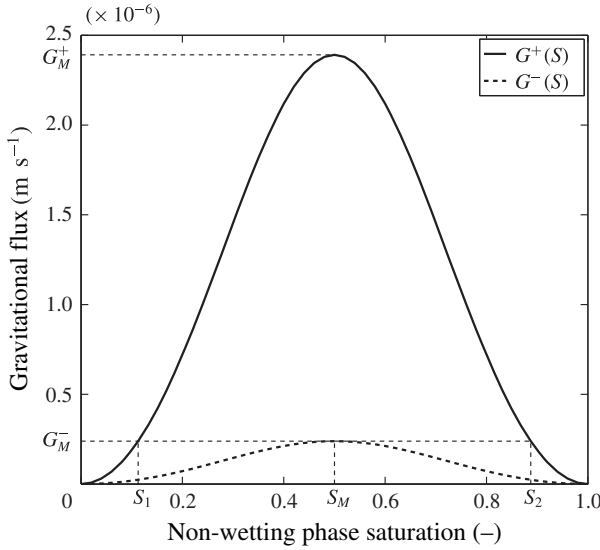


FIGURE 13. Gravitational flux curves of the layer and the matrix for  $k^-/k^+ = 1/10$ .

- (i) **C.1**:  $S_i \leq S_1$ . There is no gravity current and  $\Phi_{out} = \Phi_{in} = G(S_i)$ . The saturation in the layer is given by the buoyant flux continuity and equal to  $S_i$  on the matrix side of the upper interface of the layer.
- (ii) **C.2**:  $S_1 \leq S_i \leq S_c$ . There is a gravity current and  $\Phi_{out} = G_M^-$ . After a relaxation period, which depends on  $k^-$  the gravity current reaches a steady state. The saturation is  $S_M = 0.5$  in the layer and  $S_1$  on the matrix side of the upper interface of the layer.
- (iii) **C.3**:  $S_c \leq S_i$ . There is a gravity current but CO<sub>2</sub> flows back downwards beneath the layer and there is no steady state.

It must be remarked that the range of saturations inside which a steady state gravity current can take place,  $[S_1, S_c]$ , becomes narrow when  $k^- \rightarrow k^+$ .

Figure 14 illustrates these three cases at three different times: case **C.1** with  $S_i = 0.10$  (figures 14a–14c), case **C.2** with  $S_i = 0.15$  (figures 14d–14f) and case **C.3** with  $S_i = 0.20$  (figures 14g–14i).

The 2-D steady state CO<sub>2</sub> saturation distributions given by the model and computed using DuMu<sup>x</sup> for  $S_i = 0.15$  are depicted in figure 15, and the 1-D distributions along the vertical axis passing through the middle of the layer ( $x = 0$ ) are plotted in figure 16(a). Only the lower part of the domain is illustrated in these figures. The model and numerical results match fairly well. Particularly, we can see that the model overestimates the current height. When the layer is impermeable, the current heights are nearly identical; therefore, the observed discrepancy for the semi-permeable case is not due to the Boussinesq approximation in the gravity current model. We attribute this discrepancy to the role of the total velocity  $q_t$  (2.12), which is disregarded in our model. Because the flow is counter-current, the flow rate of the total velocity across a horizontal section is zero but the velocity is locally non-zero. The velocity increases the flux at the interface and therefore lowers the current height (figure 16b). The flux continuity at the centre ( $x = 0$ ) of the lower matrix–layer interface indicates

$$q_{mf}(S'_2) + G^+(S'_2) = q_{mf}(S'_M) + G^-(S'_M), \tag{5.3}$$

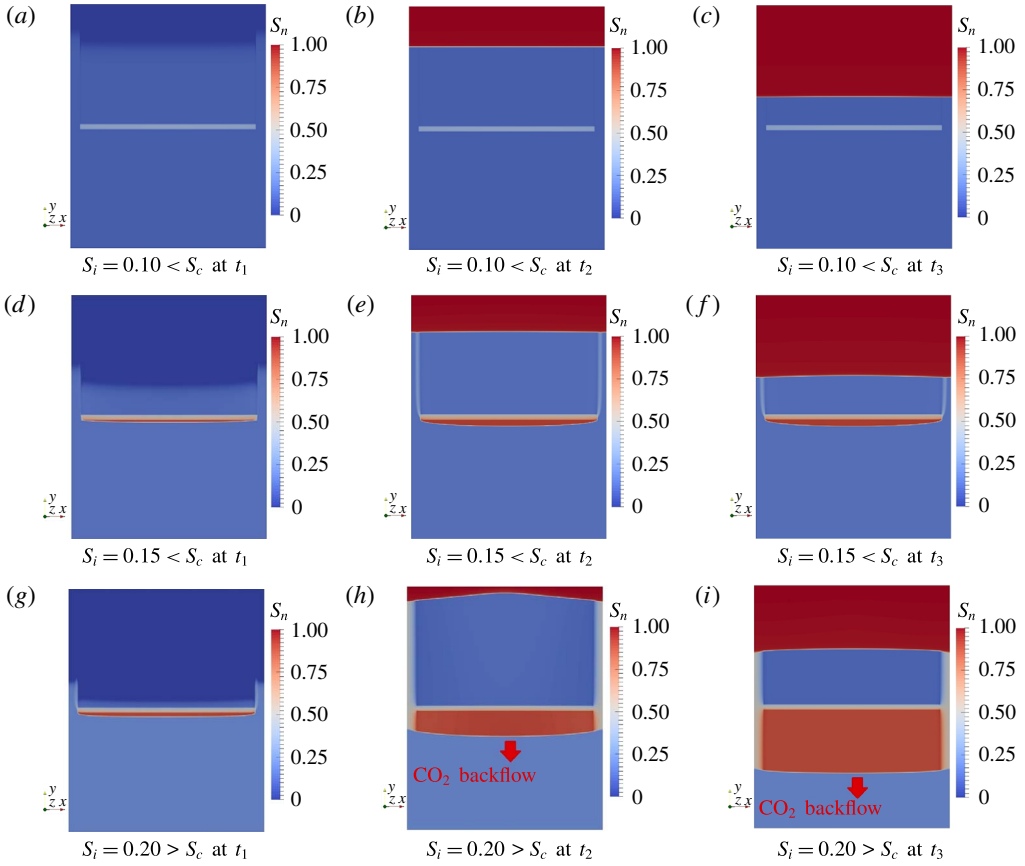


FIGURE 14. (Colour online) Capillary-free case. CO<sub>2</sub> distributions after an early time  $t_1$  (a,d,g) when the CO<sub>2</sub> plume has just reached the semi-permeable layer, at an intermediate time  $t_2$  (b,e,h) and a relatively long time  $t_3$  after the CO<sub>2</sub> plume has reached the no-flow top of the reservoir (c,f,i).

where the saturations  $S'_2$ ,  $S'_M$  are depicted in figure 16(b) and  $q_m$  is the component normal to the interface of  $\mathbf{q}_t$ . When  $\mathbf{q}_t = 0$ , we have  $S'_2 = S_2$  and  $S'_M = S_M$ . The effects of the velocity  $\mathbf{q}_t$  on the total flux continuity and the saturation discontinuity at an interface between two different porous media have been discussed by Hayek *et al.* (2009). We can graphically see that an increase in  $q_m$  increases the saturations on each side of the interface. Here, we estimate  $q_m$  from the pressure gradient  $\partial p / \partial z$  across the layer obtained numerically using DuMu<sup>x</sup>

$$q_m = -\frac{k_i}{\mu_{nw}} \left\{ [k_{r_n}(S_M)\rho_n + k_{r_w}(S_M)\rho_w]g + [k_{r_n}(S_M) + k_{r_w}(S_M)]\frac{\partial p}{\partial z} \right\}. \quad (5.4)$$

Furthermore, one obtains  $S'_M$  by solving the following nonlinear system

$$\frac{d\Phi^+}{dS} \Big|_{S'_M} = 0, \quad (5.5)$$

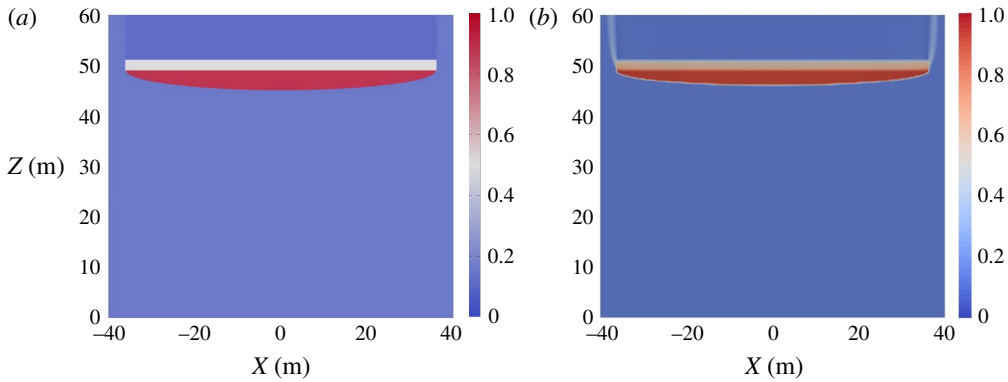


FIGURE 15. (Colour online) Capillary-free case: CO<sub>2</sub> distributions from  $Z=0$  (m) to the observation surface  $Z=60$  (m) modelled with the gravity current model (a) and simulated with DuMux (b). A moderate influx ( $S_i=0.15$ ) is imposed at the bottom of the reservoir.

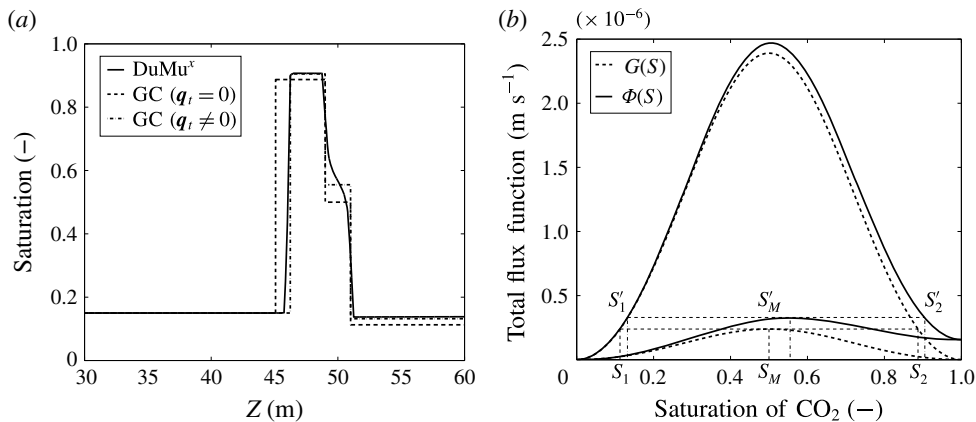


FIGURE 16. Capillary-free case: (a) CO<sub>2</sub> saturation profile along the central vertical axis of the layer. Comparison between the numerical simulation results obtained using DuMux and the analytical gravity current models, with ( $q_t \neq 0$ ) and without ( $q_t = 0$ ) the total velocity correction, for the case  $S_i=0.15$ . (b) Vertical total flux function  $\Phi(S)$  (solid line) and gravitational flux function  $G(S)$  (dotted line) at the interface between the matrix and the layer.

where  $\Phi = q_{mf}(S) + G^+(S)$ . Once  $S'_M$  is known,  $S'_2$  can be deduced from the flux continuity relationship (5.3). Here, we assume that  $\Phi(S'_M) < G^+(S_i)$  so that the flux in the layer is at its maximum value. Additionally, we assume also that the total velocity in the layer is essentially vertical, and the saturation on the matrix side of the upper layer matrix interface is  $S'_1$  (figure 16b).

Both the saturation profiles computed with and without the total velocity correction are plotted in figure 16(a). We can see that this correction significantly improves the agreement with the simulation results. This is true regardless of the imposed saturation  $S_i$  at the bottom of the domain. Figure 17 illustrates the time evolutions of the maximum current height at  $x=0$ , with (figure 17a) and without (figure 17b) the total velocity correction and for three values of  $S_i$ ,  $S_i=0.13, 0.14$  and  $0.15$ . We can

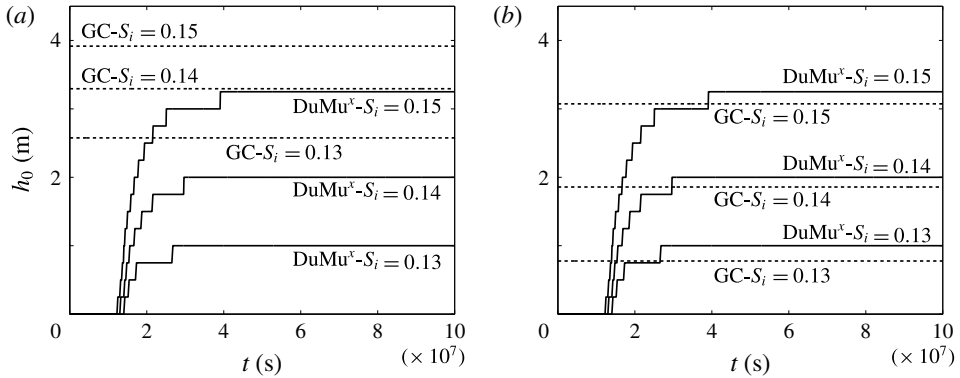


FIGURE 17. Capillary-free case: maximal gravity current height at the origin  $x = 0$ . Comparison between the numerical simulation results obtained using DuMu<sup>x</sup> (continuous lines) and the analytical gravity current models, without (a) and with (b) the total velocity.

see that ignoring the velocity results in a difference of the order of magnitude of the current height, i.e. a metre, but taking this velocity into account divides by ten the differences. These differences, showing a systematic underestimation of the model, should be improved with a refined spatial resolution.

Considering the total velocity field should improve the model; however, it is not theoretically possible. Here, the proposed correction is only applicable in the central area of the layer, where the velocity is expected to be vertical. It should be noted that we could also use an approximation of the pressure gradient, as given by flow models around thin plates. Nevertheless, at the layer extremities, the velocity in the layer is not vertical, and its impact on the total flux continuity becomes more complex to model and analyse. Thus, we disregard the velocity in the model with the capillarity discussed below.

### 5.2. Gravity-dominant case

We consider the gravity-dominant case characterized by a capillary number considerably lower than one,  $N_c \ll 1$ . The permeability ratio is set to  $k^-/k^+ = 0.10$ . This ratio results in a threshold saturation  $S_0^* = 0.90$  if the interfacial tensions of the matrix and the layer are identical. The imposed saturation at the bottom of the domain is  $S_i = 0.10$ , and only the capillarity can provoke a CO<sub>2</sub> gravity current beneath the layer. Three increasing values of the capillary number are considered:  $N_c = 0$ ,  $N_c = 0.01$  and  $N_c = 0.1$ . They correspond to increasing values of the entry pressure caused by the increase of the interfacial tension in the layer (table 1). The corresponding threshold heights of the gravity current as given by (4.9) are  $h^* = 0$  m ( $N_c = 0$ ),  $h^* = 1.054$  m ( $N_c = 0.01$ ) and  $h^* = 10.54$  m ( $N_c = 0.1$ ). Figure 18 depicts the CO<sub>2</sub> distributions obtained using DuMu<sup>x</sup> after a long time. In the capillary-free case,  $h^* = 0$ , there is no CO<sub>2</sub> accumulation beneath the barrier. The saturation within the inclusion is obtained from the continuity condition of the gravitational flux (figure 18a). When the capillary number is extremely small, i.e.  $N_c = 0.01$ , the CO<sub>2</sub> accumulation occurs because of the capillary barrier. The CO<sub>2</sub> can pass into the layer only in the zone of the interface where the gravity current height exceeds the threshold height  $h^*$ : over the zone  $-x^* \leq x \leq x^*$  with  $x^*$  being the point at which  $h = h^*$  (figure 18b). For



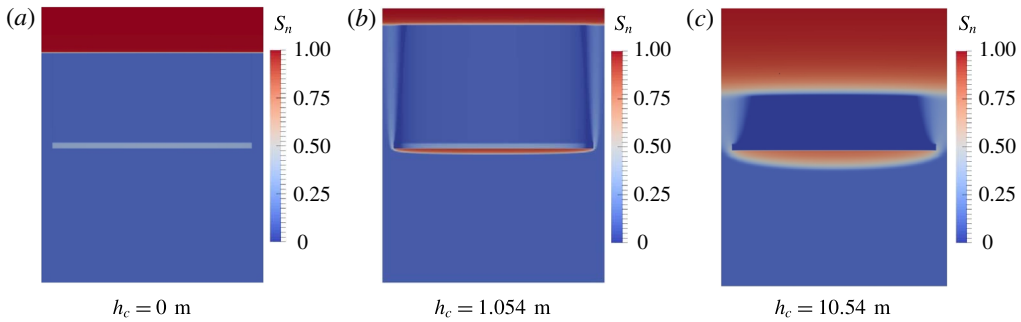


FIGURE 18. (Colour online) Gravity-dominant case with  $k^-/k^+ = 0.10$  and  $S_i = 0.10$ . The CO<sub>2</sub> saturation distributions after a long time when CO<sub>2</sub> has reached the top of the domain. The simulation results are obtained for different values of the capillary number:  $N_c = 0$  (a),  $N_c = 0.01$  (b), and  $N_c = 0.1$  (c) for which the corresponding threshold heights of the gravity current are  $h^* = 0, 1.054$  and  $10.54$ , respectively.

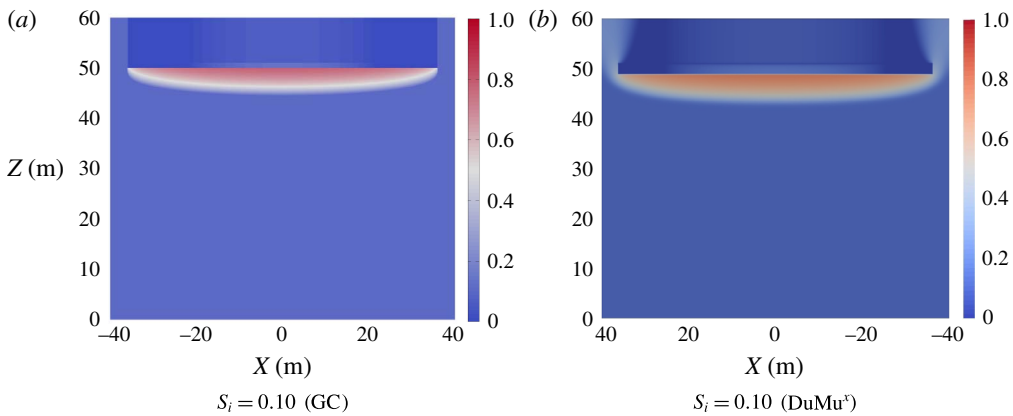


FIGURE 19. (Colour online) Gravity-dominant case with  $k^-/k^+ = 0.25$ ,  $N_c = 0.1$  and  $S_i = 0.10$ . The CO<sub>2</sub> distributions reconstructed from the semi-analytical solution (a) and simulated using DuMux (b).

a fairly high capillary number,  $N_c = 0.1$ , the threshold height  $h^*$  is also fairly high,  $h^* = 10.54$  m. Even at steady state the maximal height of the gravity current is not sufficient enough to overcome the capillary barrier (figure 18c). Therefore, the layer is impermeable to CO<sub>2</sub>.

Figure 19 depicts a comparison between the 2-D saturations in the domain computed using DuMux and reconstructed from our semi-analytical solution for  $k^+/k^- = 0.25$ ,  $S_i = 0.10$  and  $N_c = 0.1$  ( $h^* = 4.73$  m) (table 1). The two distributions agree qualitatively, and we can observe that the model accounts for the penetration of the CO<sub>2</sub> plume in a limited extent of the layer, i.e. where  $h < h^*$ .

Figure 20 illustrates the 1-D saturation distributions along the vertical axis passing through the middle of the layer and along the interface  $\Gamma$  between the matrix and the layer for two values of the imposed saturation,  $S_i = 0.10$  and  $S_i = 0.15$ . The two distributions, numerical and semi-analytical, are in good agreement for both  $S_i$

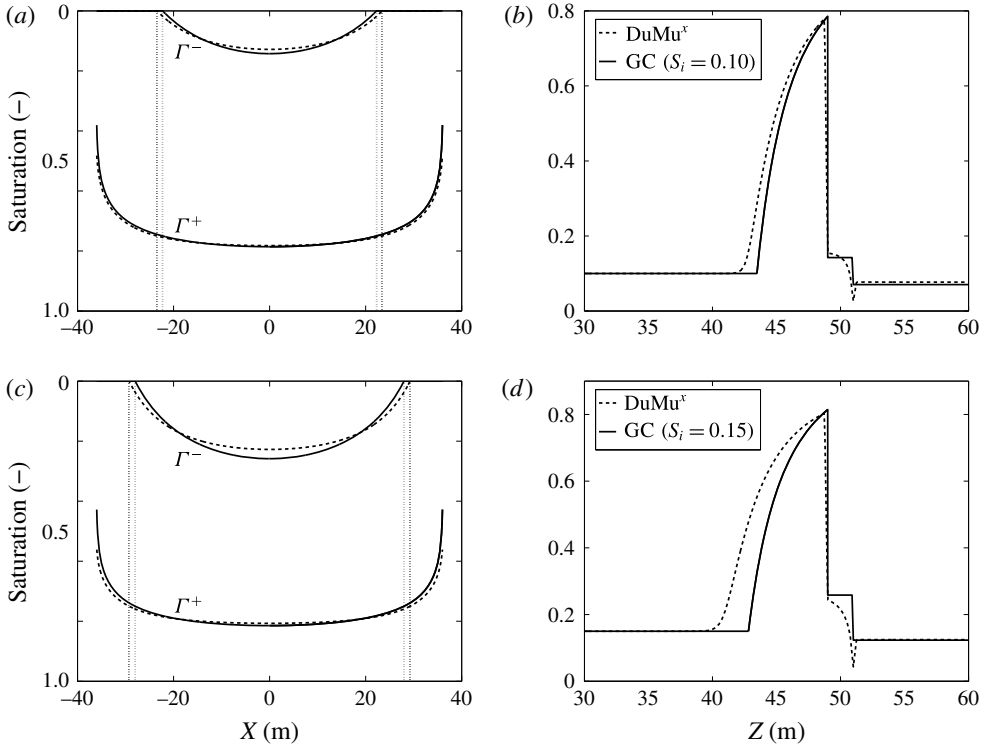


FIGURE 20. Gravity-dominant case with  $k^-/k^+ = 0.25$  and  $N_c = 0.1$ . The  $\text{CO}_2$  saturations reconstructed from the semi-analytical solution (solid line) and simulated with DuMuX (dotted line) along the horizontal interface  $\Gamma$  ( $\Gamma^-$  for the matrix side and  $\Gamma^+$  for the inclusion side) (a,c), and along the vertical central axis  $x=0$  (b,d) for the cases  $S_i = 0.10$  (a,b) and  $S_i = 0.15$  (c,d).

values. Nevertheless, a better agreement is obtained for the lowest  $S_i$  value (see the appendix A for a discussion on the impact of  $S_i$ ). The extension of the area where the  $\text{CO}_2$  can penetrate is also well described by the model (limited by the vertical dotted lines in figure 20a,c).

## 6. Summary and conclusions

We have studied by means of theoretical developments and numerical simulations the buoyancy- and capillary-driven counter-current flow of  $\text{CO}_2$  and brine through and around a semi-permeable layer of finite extent embedded in a permeable matrix. This system schematically describes the local flow of  $\text{CO}_2$  in a deep saline heterogeneous aquifer after injection has stopped or is far from the injection well. The three forces of a two-phase immiscible flow are considered: buoyancy, capillarity and viscosity.

Initially, we considered a 1-D vertical column filled with a piecewise homogeneous porous medium consisting of two materials: permeable and semi-permeable. We investigated the effects of the buoyant  $\text{CO}_2$  inflow rate on the saturation distribution in the column and for the two arrangements of the materials, that is, permeable material at the top and semi-permeable at the bottom, and the reverse. For each configuration,

we demonstrated how to graphically determine the saturation discontinuity at the interface and how the buoyant and capillary diffusion fluxes are balanced to respect the capillary pressure and total flux continuity conditions.

Then, we considered the 2-D problem. Thus, we heuristically extended the two-phase gravity current model developed by Golding *et al.* (2011) to the case of a current beneath a semi-permeable layer. The saturation in the current is imposed by the capillary pressure and the buoyant flux continuity conditions at the current layer interface. The CO<sub>2</sub> migration is therefore described by a single transport equation and the brine movement is disregarded. The numerical simulations of the system have been performed using DuMu<sup>x</sup>, an open-source simulator for the flow and transport processes in porous media developed by the University of Stuttgart (Flemisch *et al.* 2011). First, we demonstrated that for a given ratio of the layer width to the domain width, there is a threshold value of the imposed CO<sub>2</sub> saturation at the bottom of the domain, beyond which there is no steady state gravity current. An analytical estimation of this critical saturation value is proposed. Then, we compared our model to simulations in the capillary-free and gravity-dominant cases. In the gravity-dominant case, the agreement is good; the model correctly predicts the geometrical characteristics of the current and the extension of the interface region where CO<sub>2</sub> can flow into the layer, i.e. where the current height exceeds the entry pressure of the layer. In the capillary-free case, we showed that considering the total velocity in the flux at the interface significantly improves the estimation of the current characteristics. This is surprising for a counter-current flow, where the total velocity is zero in average. Nevertheless, our simulations of CO<sub>2</sub> migration in heterogeneous formations clearly indicate that in a counter-current flow or far from an injection well, the convective component of the total flux at the local interfaces of the formation plays a non-negligible role in the CO<sub>2</sub> migration. However, in both cases the model becomes less accurate when the imposed CO<sub>2</sub> saturation at the bottom of the domain, or equivalently the incoming CO<sub>2</sub> buoyant flux, increases. This saturation must be low enough, i.e. such that the associated buoyant flux is much smaller than its maximum value, to approximately respect the hydrostatic equilibrium condition in the gravity current. In the gravity-dominant case the model applies whatever the ratio of the layer permeability to the matrix permeability. In the capillary-free case this ratio must be low, less than 0.1, in order to respect the low value condition on the imposed CO<sub>2</sub> saturation. As a matter of fact, this constraint on the ratio sets to low values the range of imposed saturation inside which a steady state gravity current can take place.

The most important implication of our model for the geological storage of CO<sub>2</sub> concerns the trapping efficiency of the geological reservoir. As we discussed in the introduction, the capillary trapping is the outcome of a hysteretic process. It takes place at the trailing edge of the CO<sub>2</sub> plume during the imbibition phase, i.e. after injection has stopped (Doughty 2007; Hesse *et al.* 2008). If the reservoir is initially free of CO<sub>2</sub>, i.e. before injection, the trapped mass gives the CO<sub>2</sub> initial residual saturation, and also new characteristic curves, if another injection takes place. This mass depends on the total volume of reservoir swept by the plume. When capillarity is neglected and layers are semi-permeable the plume should invade a large volume of the reservoir, much larger than if the layers are impermeable. According to Land's model, used for instance by Juanes *et al.* (2006) for applications to CO<sub>2</sub> sequestration reservoirs, residual saturations slightly smaller than the imposed saturations considered here (0.10–0.15) are expected in the 2-D layer matrix reservoir. When capillarity is taken into account and layers are perfect capillary barriers

Golding *et al.* (2011) showed that, compared to the capillary-free case, capillary diffusion can decrease by a factor of 2 the fraction of CO<sub>2</sub> trapped in the gravity current. If the layers are imperfect capillary barriers, i.e. CO<sub>2</sub> can overcome locally the barrier, the use of a numerical code becomes a necessity to assess this efficiency. The other trapping mechanism, dissolution, should also be enhanced by the presence of semi-permeable layers as its importance depends on the contact volume between CO<sub>2</sub> and brine.

Lastly, we would like to emphasize that our results may be easily applied to the problem of groundwater contamination by DNAPL (Dense Non Aqueous Phase Liquid) or LNAPL (Light Non aqueous Phase Liquid). The physical problems are identical to that of CO<sub>2</sub>: (i) the DNAPL migrates downwards, whereas the LNAPL upwards, both of which driven by the difference in the density with the aquifer interstitial water; and (ii) the heterogeneities of a subsurface aquifer are frequently of the semi-permeable type (Helmig 1997).

### Acknowledgements

This study was supported by the project H-CUBE (Hydrodynamics, Heterogeneity, and Homogenization) of the French National Agency of Research (ANR).

### Appendix A

In this appendix we provide several theoretical elements that support the extension to semi-permeable layers of the two-phase gravity current model of Golding *et al.* (2011) exposed in §4.

First, let us neglect capillarity and consider a 1-D vertical column filled with two homogeneous porous media: a permeable matrix and a semi-permeable layer of height  $\delta$  located at the centre of the column. The absolute permeabilities of the matrix and the layer are respectively  $k^+$  and  $k^-$ . A constant saturation  $S_i$  is imposed at the bottom of the column initially filled with brine (same configuration as in §3) and flow is counter-current. Following the discussion of §3, and more generally the results exposed in (Hayek *et al.* 2009), we see that if  $S_i < S_M$ , where  $S_M$  is the saturation at which the buoyant flux is maximum (figure 13), the plume can cross the layer and the steady state saturation in the layer  $S_l$  is given by the buoyant flux continuity,  $G^-(S_l) = G^+(S_l)$  where  $G^+$  and  $G^-$  are the buoyant flux functions of the matrix and the layer respectively (2.17). Flux continuity shows also that the saturation at steady state above the layer is  $S_i$ . We assume here that  $S_i$  is lower than the Welge saturation,  $S_w \approx 0.4$  here, so that the saturations in the lower and upper parts part of the column are described as shock waves (Hayek *et al.* 2009). If  $S_i > S_M$  all the incoming flux cannot penetrate into the layer and an unsteady accumulation takes place beneath the lower interface of the layer. Again, flux continuity shows that the saturation is  $S_2$  in the accumulation zone,  $S_M$  in the layer and  $S_1$  above the layer where  $G^+(S_1) = G^+(S_2) = G^-(S_M)$  ( $S_1 < S_2$ ) (figure 13). The width of the accumulation zone increases with time and the front of this zone is described as a shock travelling downwards. One must note that when  $k^- \rightarrow 0$ ,  $S_2 \rightarrow 1$ ,  $S_1 \rightarrow 0$  and  $S_l = S_M$ . From the counter-current flow condition,  $q_t = 0$ , it is easy to obtain the pressure gradient in the column

$$\frac{\partial p}{\partial z} = -\varphi(S)g, \quad \varphi(S) = \frac{\rho_{nw}\lambda_{nw}(S) + \rho_w\lambda_w(S)}{\lambda_{nw}(S) + \lambda_w(S)}, \quad (\text{A } 1a,b)$$

where  $\lambda_\alpha(S) = k_{r\alpha}(S)/\mu_\alpha$  is the mobility of fluid  $\alpha$  ( $\alpha = nw, w$ ). After integration, the pressure in the accumulation zone is

$$p(z, t) = p_0(z) + [\varphi(S_i) - \varphi(S_2)]gh(t), \tag{A 2}$$

where  $p_0(z)$  is a pressure depending on  $z$  only and  $h(t)$  is the thickness of the accumulation zone at time  $t$ . This thickness linearly increases with time with a velocity  $G^+(S_2)/S_2$ .

If we now introduce a second dimension to the problem, i.e. the vertical 1-D column becomes the 2-D system described in § 4, the accumulation can spread laterally, the velocity of the shock travelling downwards in one dimension tends to zero and the excess of influx is balanced by a spreading flux beneath the layer. We assume that the physics of this 2-D problem can be approximated as a vertical 1-D problem where saturations are governed by buoyant flux continuity conditions at the two interfaces between the matrix and layer and a 1-D spreading problem along the horizontal axis governed by the horizontal pressure gradient in the accumulation zone, i.e. the gravity current. As the saturation is constant along the vertical of the accumulation zone the spreading flow rate may be written

$$Q_x = -k^+ \lambda_{nw}(S_2)h \frac{\partial p}{\partial x}. \tag{A 3}$$

When  $k^- \rightarrow 0$ ,  $p \rightarrow [\varphi(S_i) - \rho_{nw}] gh/\mu_{nw}$ . This expression is different of the classical gravity current pressure because the brine and the CO<sub>2</sub> are in movement; the two fluids cannot be in the hydrostatic equilibrium. When  $S_i \approx 0$  one can approximate  $p \simeq \Delta\rho gh/\mu_{nw}$  which is the classical expression of the gravity current pressure. In our 2-D gravity current model for a semi-permeable layer,  $S_i$  is small,  $S_i \approx 0.1$ , and  $k^-/k^+ \ll 1$  which leads to a value of  $S_2$  close to one. Therefore, we assume, as a first approximation, that the previous expression of the gravity current pressure can be used. It is worth to remark that the values of the gravity current saturation simulated with DuMu<sup>+</sup> for semi permeable layers of permeability  $k^-/k^+ = 0.1$  and  $0.25$  (§ 4) are in good agreement with their respective  $S_2$  values.

When capillarity is taken into account and the physical parameters of the 2-D problem are such that the layer is a capillary barrier (§ 5.2) the model of Golding *et al.* (2011) applies if  $S_i$  is small,  $\simeq 0.1$ . This constraint, which is the same as in the capillary-free case treated previously, must be introduced to approximately respect the hydrostatic equilibrium condition in each phase. For this same reason  $S_i$  must also be small when the layer is not a capillary barrier. According to the notations of (§ 3.1) the flux continuity condition at the lower matrix–layer interface is

$$G^+(S_i) = G^+(S_L) - D^+(S_L) \left. \frac{\partial S}{\partial z} \right|_{S_L}, \tag{A 4}$$

where  $D(S) = N_c \sqrt{k^+} \Lambda(S) J'_s$  is the capillary diffusion coefficient (3.4). When  $S_i \rightarrow 0$  the case of an impermeable layer described by Golding *et al.* (2011) is recovered. Figure 21 shows a comparison between the 1-D steady state saturations computed using a home-made code and the model. The system is the 1-D column filled with the piecewise homogeneous porous medium studied in § 3. We see that the model converges to the numerical solution when  $S_i \rightarrow 0$  and the error is low when  $S_i$  is close to, or smaller than 0.1. This figure also illustrates the equality given in (A 4): the diffusive flux at the interface given by the model underestimates the numerical one.

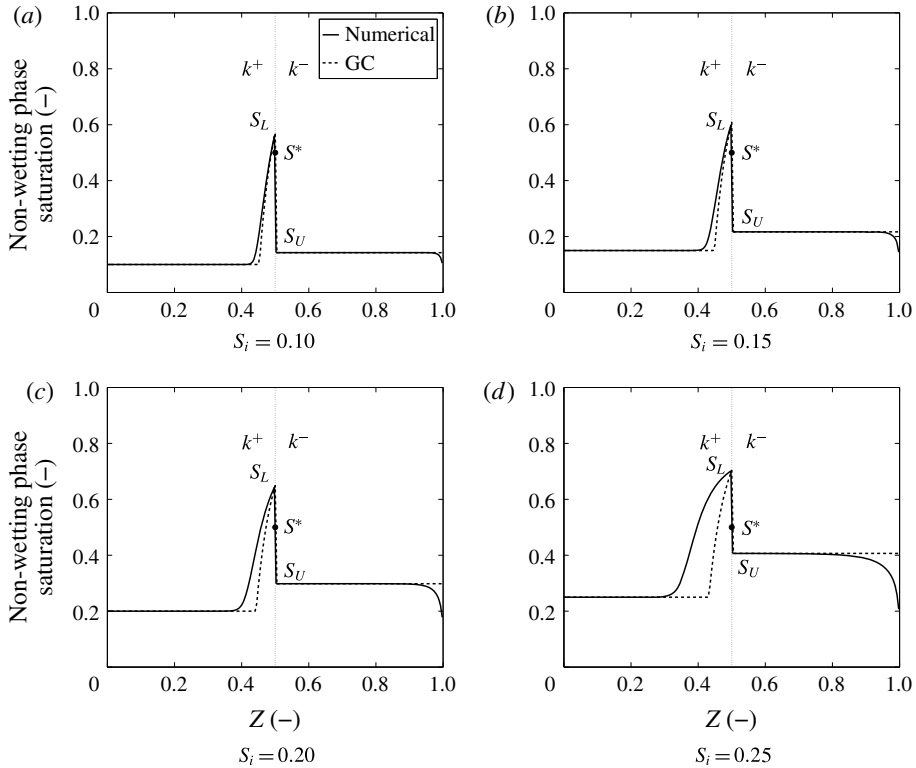


FIGURE 21. Piecewise homogeneous porous medium column. Saturation distributions predicted by the model and computed with a home-made code for four values of the imposed saturation  $S_i$ .

#### REFERENCES

- ACTON, J. M., HUPPERT, H. E. & WORSTER, M. 2001 Two-dimensional viscous gravity currents flowing over a deep porous medium. *J. Fluid Mech.* **440**, 359–380.
- ADIMURTHI, JAFFRÉ, J. & VEERAPPA GOWDA, G. D. 2004 Godunov-type methods for conservation laws with a flux function discontinuous in space. *SIAM J. Numer. Anal.* **42** (1), 179–208.
- AMBROSE, W. A., LAKSHMINARASIMHAN, S., HOLTZ, M. H., NUNEZ-LOPEZ, V., HOVORKA, S. D. & DUNCAN, I. 2008 Geologic factors controlling CO<sub>2</sub> storage capacity and permanence: case studies based on experience with heterogeneity in oil and gas reservoirs applied to CO<sub>2</sub> storage. *Environ. Geol.* **54** (8), 1619–1633.
- AMES, W. F. 2014 *Numerical Methods for Partial Differential Equations*. Academic.
- ANDREIANOV, B. & CANCEÈS, C. 2013 Vanishing capillarity solutions of buckley–leverett equation with gravity in two-rocks' medium. *Comput. Geosci.* **17** (3), 551–572.
- BEAR, J. 1988 *Dynamics of Fluids in Porous Media*. Dover.
- BENSON, S., COOK, P., ANDERSON, J., BACHU, S., NIMIR, H. B., BASU, B., BRADSHAW, J., DEGUCHI, G., GALE, J., VON GOERNE, G. *et al.* 2005 Underground geological storage. In *IPCC Special Report on Carbon Dioxide Capture and Storage*, pp. 195–276.
- BICKLE, M., CHADWICK, A., HUPPERT, H. E., HALLWORTH, M. & LYLE, S. 2007 Modelling carbon dioxide accumulation at Sleipner: implications for underground carbon storage. *Earth Planet. Sci. Lett.* **255** (1), 164–176.
- BROOKS, R. H. & COREY, A. T. 1964 Hydraulic properties of porous media. In *Hydrology Papers*, Colorado State University.

- BRYANT, S. L., LAKSHMINARASIMHAN, S. & POPE, G. A. 2008 Buoyancy-dominated multiphase flow and its effect on geological sequestration of CO<sub>2</sub>. *SPE J.* **13** (04), 447–454.
- BUZZI, F., LENZINGER, M. & SCHWEIZER, B. 2009 Interface conditions for degenerate two-phase flow equations in one space dimension. *Anal. Intl Math. J. Anal. Appl.* **29** (3), 299–316.
- CANCÈS, C. 2008 Two-phase flows in heterogeneous porous media: modeling and analysis of the flows of the effects involved by the discontinuities of the capillary pressure. PhD thesis, Université de Provence – Aix – Marseille I.
- CANCÈS, C. 2010a Asymptotic behavior of two-phase flows in heterogeneous porous media for capillarity depending only on space. I. Convergence to the optimal entropy solution. *SIAM J. Math. Anal.* **42** (2), 946–971.
- CANCÈS, C. 2010b Asymptotic behavior of two-phase flows in heterogeneous porous media for capillarity depending only on space. II. Non classical shocks to model oil-trapping. *SIAM J. Math. Anal.* **42** (2), 972–995.
- CANCÈS, C., GALLOUËT, T. & PORRETTA, A. 2009 Two-phase flows involving capillary barriers in heterogeneous porous media. *Interfaces Free Bound.* **11**, 239–258.
- CELIA, M. A., BACHU, S., NORDBOTTEN, J. M. & BANDILLA, K. W. 2015 Status of CO<sub>2</sub> storage in deep saline aquifers with emphasis on modeling approaches and practical simulations. *Water Resour. Res.* **51** (9), 6846–6892.
- DOUGHTY, C. 2007 Modeling geologic storage of carbon dioxide: comparison of non-hysteretic and hysteretic characteristic curves. *Energy Convers. Manage.* **48** (6), 1768–1781.
- FLEMISCH, B., DARCIS, M., ERBERTSEDER, K., FAIGLE, B., LAUSER, A., MOSTHAF, K., MÜTHING, S., NUSKE, P., TATOMIR, A., WOLFF, M. *et al.* 2011 DuMu<sup>x</sup>: DUNE for multi-{phase, component, scale, physics, . . .} flow and transport in porous media. *Adv. Water Resour.* **34** (9), 1102–1112.
- GOLDING, M. J., HUPPERT, H. E. & NEUFELD, J. A. 2013 The effects of capillary forces on the axisymmetric propagation of two-phase, constant-flux gravity currents in porous media. *Phys. Fluids* **25** (3), 036602.
- GOLDING, M. J., NEUFELD, J. A., HESSE, M. A. & HUPPERT, H. E. 2011 Two-phase gravity currents in porous media. *J. Fluid Mech.* **678**, 248–270.
- HAYEK, M., MOUCHE, M. & MÜGLER, C. 2009 Modeling vertical stratification of CO<sub>2</sub> injected into a deep layered aquifer. *Adv. Water Resour.* **32** (3), 450–462.
- HELMIG, R. 1997 *Multiphase Flow and Transport Processes in the Subsurface: a Contribution to the Modeling of Hydrosystems*. Springer.
- HESSE, M. A., ORR, F. M. & TCHELEPI, H. A. 2008 Gravity currents with residual trapping. *J. Fluid Mech.* **611**, 35–60.
- HESSE, M. A., TCHELEPI, H. A., CANTWEL, B. J. & ORR, F. M. 2007 Gravity currents in horizontal porous layers: transition from early to late self-similarity. *J. Fluid Mech.* **577**, 363–383.
- HESSE, M. A. & WOODS, A. W. 2010 Buoyant dispersal of CO<sub>2</sub> during geological storage. *Geophys. Res. Lett.* **37** (1), L01403.
- HONARPOUR, M. M., KOEDERITZ, F. & HERBERT, A. 1986 *Relative Permeability of Petroleum Reservoirs*. CRC.
- HUPPERT, H. E. & NEUFELD, J. A. 2014 The fluid mechanics of carbon dioxide sequestration. *Annu. Rev. Fluid Mech.* **46**, 255–272.
- HUPPERT, H. E. & WOODS, A. W. 1995 Gravity-driven flows in porous layers. *J. Fluid Mech.* **292**, 55–69.
- JUANES, R., MACMINN, C. W. & SZULCZEWSKI, M. L. 2010 The footprint of the CO<sub>2</sub> plume during carbon dioxide storage in saline aquifers: storage efficiency for capillary trapping at the basin scale. *Transp. Porous Med.* **82** (1), 19–30.
- JUANES, R., SPITERI, E. J., ORR, F. M. & BLUNT, M. J. 2006 Impact of relative permeability hysteresis on geological CO<sub>2</sub> storage. *Water Resour. Res.* **42** (12).
- KAASSCHIETER, E. F. 1999 Solving the buckley-leverett equation with gravity in a heterogeneous porous medium. *Comput. Geosci.* **3** (1), 23–48.

- LANGTANGEN, H. P., TVEITO, A. & WINTHER, R. 1992 Instability of Buckley-Leverett flow in a heterogeneous medium. *Trans. Porous Med.* **9** (3), 165–185.
- LENGLER, U., DE LUCIA, M. & KÜHN, M. 2010 The impact of heterogeneity on the distribution of CO<sub>2</sub>: numerical simulation of CO<sub>2</sub> storage at Ketzin. *Intl J. Greenh. Gas Control* **4** (6), 1016–1025.
- LYLE, S., HUPPERT, H. E., HALLWORTH, M., BICKLE, M. & CHADWICK, A. 2005 Axisymmetric gravity currents in a porous medium. *J. Fluid Mech.* **543**, 293–302.
- MIKELIC, A., VAN DUIJN, C. & POP, I. 2002 Effective equations for two-phase flow with trapping on the micro scale. *SIAM J. Appl. Maths* **62** (5), 1531–1568.
- NEUFELD, J. A. & HUPPERT, H. E. 2009 Modelling carbon dioxide sequestration in layered strata. *J. Fluid Mech.* **625**, 353–370.
- NORDBOTTEN, J. M. & CELIA, M. A. 2006 Similarity solutions for fluid injection into confined aquifers. *J. Fluid Mech.* **561**, 307–327.
- PRITCHARD, D., WOODS, A. W. & HOGG, A. J. 2001 On the slow draining of a gravity current moving through a layered permeable medium. *J. Fluid Mech.* **444**, 23–47.
- SPANNUTH, M. J., NEUFELD, J. A., WETTLAUFRER, J. S. & WORSTER, M. 2009 Axisymmetric viscous gravity currents flowing over a porous medium. *J. Fluid Mech.* **622**, 135–144.
- VAN DUIJN, C. J. & DE NEEF, M. J. 1998 Similarity solution for capillary redistribution of two phases in a porous medium with a single discontinuity. *Adv. Water Resour.* **21** (6), 451–461.
- VAN DUIJN, C. J., MOLENAAR, J. & DE NEEF, M. J. 1995 The effect of capillary forces on immiscible two-phase flow in heterogeneous porous media. *Trans. Porous Med.* **21** (1), 71–93.
- VAN GENUCHTEN, M. TH. 1980 A closed-form equation for predicting the hydraulic conductivity of unsaturated soils. *Soil Science Soc. Am. J.* **44** (5), 892–898.
- VELLA, D. & HUPPERT, H. E. 2006 Gravity currents in a porous medium at an inclined plane. *J. Fluid Mech.* **555**, 353–362.
- WOODS, A. W. & FARCAS, A. 2009 Capillary entry pressure and the leakage of gravity currents through a sloping layered permeable rock. *J. Fluid Mech.* **618**, 361–379.